Palaeogeography, Palaeoclimatology, Palaeoecology 613 (2023) 111412

Contents lists available at ScienceDirect

Palaeogeography, Palaeoclimatology, Palaeoecology

journal homepage: www.elsevier.com/locate/palaeo

Volcanism and carbon cycle perturbations in the High Arctic during the Late Jurassic – Early Cretaceous

Madeleine L. Vickers [a,*], Mads E. Jelby [b], Kasia K. Śliwińska [c], Lawrence M.E. Percival [d], Feiyue Wang [e], Hamed Sanei [f], Gregory D. Price [g], Clemens V. Ullmann [h], Stephen E. Grasby [j], Lutz Reinhardt [k], Tamsin A. Mather [i], Joost Frieling [i], Christoph Korte [b], Rhodri M. Jerrett [l], Morgan T. Jones [a], Ivar Midtkandal [m], Jennifer M. Galloway [j,n]

[a] Centre for Earth Evolution and Dynamics (CEED), University of Oslo, P.O. Box 1028 Blindern, 0315 Oslo, Norway
[b] Department of Geosciences and Natural Resource Management, University of Copenhagen, Øster Voldgade 10, DK-1350 Copenhagen K, Denmark
[c] Geological Survey of Denmark and Greenland (GEUS), Department of Geoenergy and Storage, Øster Voldgade 10, DK-1350 Copenhagen K, Denmark
[d] Analytical, Environmental and Geochemistry Group (AMGC), Pleinlaan 2, Vrije Universiteit Brussel, 1050 Brussels, Belgium
[e] Centre for Earth Observation Science and Department of Environment and Geography, University of Manitoba, Winnipeg, MB R3T 2N2, Canada
[f] Department of Geoscience, Aarhus University, Høegh-Guldbergs Gade 2, DK-8000 Aarhus C, Denmark
[g] School of Geography, Earth and Environmental Sciences, Plymouth University, Drake Circus, Plymouth PL4 8AA, UK
[h] Camborne School of Mines, University of Exeter, Penryn Campus, Penryn, Cornwall TR10 9FE, UK
[i] Department of Earth Sciences, University of Oxford, Oxford OX1 3AN, UK
[j] Geological Survey of Canada, 3303 33rd St N.W., Calgary, Alberta T2L 2A7, Canada
[k] Bundesanstalt für Geowissenschaften und Rohstoffe (BGR), Federal Institute for Geosciences and Natural Resources, Geozentrum Hannover, Stilleweg 2, D-30655 Hannover, Germany
[l] School of Earth and Environmental Sciences, University of Manchester, Oxford Road, Manchester M13 9PL, UK
[m] Department of Geosciences, University of Oslo, P.O. Box 1047, Blindern, 0315 Oslo, Norway
[n] Aarhus Institute of Advanced Studies, Aarhus University, Høegh-Guldbergs Gade 6B, DK-8000 Aarhus C, Denmark

ARTICLE INFO

Editor: A Dickson

Keywords:
CIEs
VOICE
Weissert Event
Mercury
Ocean Anoxic Event 1a
HALIP
Ontong-Java Plateau

ABSTRACT

Large perturbations in the global carbon cycle recorded as carbon-isotope ($\delta^{13}C$) excursions (CIEs) in both organic carbon and carbonate records have been linked to volcanism during the emplacement of Large Igneous Provinces (LIPs). This link is based primarily on the purported temporal coincidence between CIEs and LIP emplacement. Mercury (Hg) concentration in sedimentary rocks has been used as a regional to global tracer of large-scale volcanic activity, yet few studies have been undertaken on Upper Jurassic – Lower Cretaceous sediments from Boreal localities compared to those for Tethyan (northern mid-latitude) successions. This has limited our understanding of the regional-to-global spatial impact of volcanic activity during this period. This study examines the Hg record as a proxy for volcanism, and the $\delta^{13}C$ records from organic matter ($\delta^{13}C_{org}$) of CIEs from the uppermost Jurassic to Lower Cretaceous (Callovian – Aptian) successions from Axel Heiberg and Spitsbergen in the Canadian Arctic and Svalbard archipelagos, respectively. This interval includes three regional- to global CIEs. These sections show no significant variation in the ratio of Hg to total organic carbon (TOC) across the Boreal-wide Volgian negative CIE (Volgian Isotopic Carbon Excursion, "VOICE"), which has not been associated with LIP volcanism. The examined successions spanning this interval all show some influence from changing environmental or post-burial parameters, however, which could have (partially) overprinted a volcanic signal. Despite some problems in stratigraphically constraining the Weissert Event, increased Hg/TOC ratios are observed across this interval, which may be partially driven by volcanism associated with the emplacement of the Paraná-Etendeka Traps. A spike in Hg/TOC is observed immediately prior to the negative peak of the Aptian Oceanic Anoxic Event (OAE1a) CIE, supporting recent evidence of a pulse of High Arctic Large Igneous Province (HALIP) volcanic activity preceding this oceanic anoxic event.

* Corresponding author.
E-mail address: m.l.vickers@geo.uio.no (M.L. Vickers).

https://doi.org/10.1016/j.palaeo.2023.111412
Received 26 July 2022; Received in revised form 31 December 2022; Accepted 13 January 2023
Available online 24 January 2023

1. Introduction

The long-term greenhouse conditions that prevailed during the Mesozoic were punctuated by episodes of major climate and environmental change, recorded as global perturbations in stable oxygen ($\delta^{18}O$) and carbon ($\delta^{13}C$) isotope records and often associated with elevated organic matter in the sedimentary record (Robinson et al., 2017). Some of the larger climatic disturbances have been linked to the emplacement of Large Igneous Provinces (LIPs), based on a temporal correlation between the ages of LIP rocks, carbon-isotope excursions (CIEs) and biotic change that suggests a potential causal connection (e.g. Coffin and Eldholm, 1994; Courtillot and Renne, 2003; Weissert and Erba, 2004; Ernst, 2014; Bond and Grasby, 2017; Kasbohm et al., 2021). For the early Cretaceous LIPs and CIEs, numerous studies have been undertaken on mid- and low-latitude sediments deposited during these events (e.g. Coffin and Eldholm, 1994; Courtillot and Renne, 2003; Weissert and Erba, 2004; Ernst, 2014; Bond and Grasby, 2017; Kasbohm et al., 2021), but there has been comparatively little investigation of higher palaeolatitude sites (Hammer et al., 2012; Jelby et al., 2020a; Galloway et al., 2020, 2022), which must be examined to test if observed trends in any of the proxies examined are indeed global in extent. Sedimentary successions spanning the uppermost Jurassic and most of the Lower Cretaceous (Callovian – Aptian, c. 165–113 Ma) outcrop in the Canadian Arctic and Svalbard archipelagos. This interval includes three regional- to global-scale carbon isotope excursions (CIEs). In the uppermost Jurassic, an Boreal-wide CIE, known as the Volgian Isotopic Carbon Excursion (VOICE), is recognised (e.g. Hammer et al., 2012; Galloway et al., 2020; Jelby et al., 2020a). Lower Cretaceous Arctic sediments document two further CIEs, which are observed in both carbonate and organic carbon records from the Berriasian to Aptian worldwide, namely the Valanginian Weissert Event and the early Aptian Oceanic Anoxic Event (OAE1a) (e.g. Jenkyns, 1980; Weissert et al., 1998; Erba et al., 2004; Bodin et al., 2015; Herrle et al., 2015; Vickers et al., 2016; Galloway et al., 2020). Each of these CIEs has their own unique characteristics, and the mechanisms by which they occurred were likely different, as detailed below.

1.1. The VOICE event

Boreal records display a strong negative CIE in uppermost Jurassic strata, of c. 5 ‰ (e.g. Galloway et al., 2020; Jelby et al., 2020a and references therein). This excursion marks the VOICE event (Hammer et al., 2012; Koevoets et al., 2016; Galloway et al., 2020), roughly spanning the Tithonian/Volgian (Jelby et al., 2020a), from c. 149–142 Ma; Gradstein et al., 2020). Low- and mid-latitude (i.e. Tethyan and Pacific) carbonate carbon isotope records ($\delta^{13}C_{carb}$) show a gradual decreasing trend from the uppermost Jurassic to Lower Cretaceous, with no significant perturbations until the positive CIE of the Weissert Event (Price et al., 2016). The VOICE is believed to have arisen due to isolation of the Boreal oceans leading to the compositional evolution away from open-marine carbon isotopic values (Galloway et al., 2020; Jelby et al., 2020a). Such separation of the Boreal carbon reservoirs from those the global oceans is thought to have been driven by a eustatic sea-level lowstand isolating the Boreal basins during the latest Jurassic, followed by eustatic sea-level rise in the earliest Cretaceous that led to a recoupling of these carbon reservoirs in the Valanginian (Galloway et al., 2020; Jelby et al., 2020a). Such basin isolation has led to pronounced oceanic species provincialism, resulting in ongoing challenges in correlating the Boreal regional stages to international stages across the Jurassic – Cretaceous boundary, and the persistent usage of Boreal-specific stage names (e.g. “Volgian, Ryazanian”) (Gradstein et al., 2020).

The Jurassic–Cretaceous transition was also marked by the emplacement of the Shatsky Rise plateau in the northwest Pacific Ocean (Fig. 1; Mahoney et al., 2005; Sager et al., 2013; Geldmacher et al., 2014). It is unclear how much this volcanic event may have influenced Earth’s climate and/or global to local carbon cycle changes.

1.2. The Weissert Event

The Weissert Event positive CIE is recognised in both terrestrial and marine records across the globe in the late Valanginian to early Hauterivian (e.g. Weissert et al., 1998; Erba et al., 2004; Gröcke et al., 2005), although there is much debate about the exact timing of this event (Gradstein et al., 2020). The Weissert Event is hypothesised to reflect increased burial of isotopically light (^{13}C-depleted) carbon (organic matter), and/or reduction of the isotopically heavier carbon reservoir (carbonate). The triggers and mechanism for the Weissert Event CIE are debated, but it is widely believed that increased atmospheric CO_2 would have enhanced hydrological cycling, and thus increased weathering and nutrient discharge to global oceans (Weissert and Erba, 2004; Duchamp-Alphonse et al., 2007; Gréselle et al., 2011). Nutrient input such as this would have effectively fertilised the ocean and caused an increase primary productivity, which could lead to the development of oxygen-deficient conditions and a higher rate of organic matter burial in seafloor sediments. The rise in CO_2 required to drive such changes in the hydrological cycle could have been sourced from volcanic carbon emissions (e.g. Weissert et al., 1998; Weissert and Erba, 2004; Duchamp-Alphonse et al., 2007; Charbonnier et al., 2017). The Weissert Event was

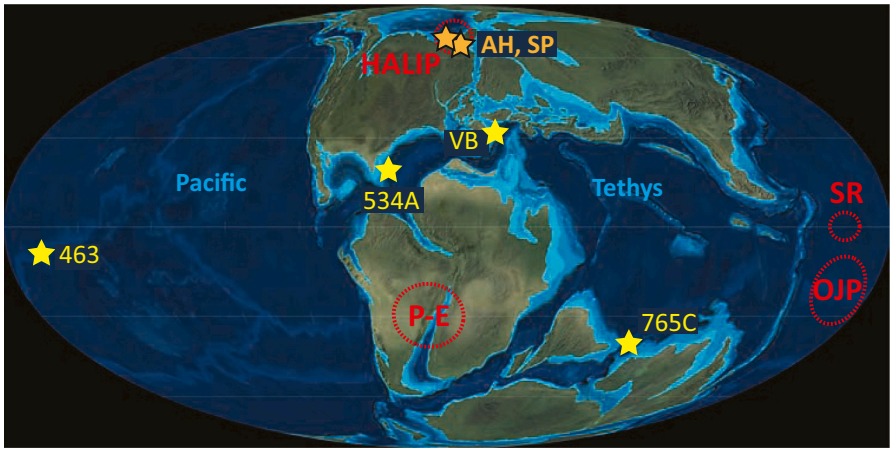

Fig. 1. Volcanic centres in relation to studied sites on a palaeogeographic reconstruction for the earliest Cretaceous (c. 140 Ma). Modified from Charbonnier et al. (2020b) after Blakey (2020); http://cpgeosystems.com/euromaps.html). AH = Axel Heiberg, Sp. = Spitsbergen; VB—Vocontian Basin; PB—Polish Basin; UM = Umbria-Marche Basin; HALIP = High Arctic Large Igneous Province; SR = Shatsky Rise; OJP = Greater Ontong Java Plateau; P-E = Paranà -Etendeka Traps.

broadly coeval with the emplacement of the Paraná-Etendeka LIP (Fig. 1; e.g. Weissert and Erba, 2004; Duchamp-Alphonse et al., 2007; Martinez et al., 2015; Gomes and Vasconcelos, 2021), a large-scale emplacement of igneous rocks on continental crust that occurred during the rifting between the South American and African plates (Peate, 1997; Hawkesworth et al., 2000). However, the magnitude of climatic effects resulting from Paraná-Etendeka volcanism was small compared to its size (e.g. Ganino and Arndt, 2009; Jones et al., 2016), and there is limited evidence for climate warming during the Weissert Event compared to other episodes of environmental change associated with LIPs (e.g. Cavalheiro et al., 2021;Littler et al., 2011;McArthur et al., 2007;Price and Passey, 2013). The Paraná-Etendeka traps were emplaced in a sub-tropical arid environment (e.g. Waichel et al., 2008), so the weathering and erosion that would have supplied much of the nutrients and alkalinity to the ocean were much diminished (Jones et al., 2016), countering the theory for this alone causing the widespread fertilization and increased productivity of the oceans that resulted in the Weissert Event CIE. Moreover, the exact temporal relationship between the Weissert Event and emplacement of the Paraná-Etendeka traps remains debated, with volcanism hypothesised to have occurred gradually over several million years at a slower pace than many other continental LIPs (Dodd et al., 2015), and with a major pulse of eruptions post-dating the onset of the carbon-cycle perturbation (Rocha et al., 2020).

1.3. Ocean Anoxic Event 1a (OAE1a)

The globally-recognised early Aptian CIE (c. 120 Ma; Gradstein et al., 2020) is associated with widespread black shale deposition (e.g. Sliter, 1989; Bralower et al., 1994; Mutterlose et al., 2009) and is considered to mark an Oceanic Anoxic Event, known as OAE1a (Jenkyns, 1980). In $\delta^{13}C$ records, OAE1a is expressed as a sharp negative CIE followed by a double-peaked positive "recovery" CIE that is recorded globally in both terrestrial and marine organic and carbonate carbon records (Jenkyns, 1995; Menegatti et al., 1998; Ando et al., 2002; Price, 2003; Weissert and Erba, 2004; Herrle et al., 2015). There are two LIPs which were emplaced around the same time as OAE1a. The Greater Ontong-Java Plateau, formed in the western Pacific Ocean primarily through submarine volcanism, represents the largest preserved LIP known on Earth (Fig. 1; Tarduno et al., 1991; Erba et al., 1999, 2015; Chambers et al., 2004; Thordarson, 2004; Kerr and Mahoney, 2007; Tejada et al., 2009; Percival et al., 2021a). The Ontong-Java Plateau alone likely has a crustal volume of c. 50 million km^3 (Gladczenko et al., 1997), potentially supplemented by additional magmas on the Manihiki and Hikurangi plateaus that may have also formed as part of the Greater Ontong-Java Plateau (Taylor, 2006; Hoernle et al., 2010). Moreover, if a part of the Greater Ontong-Java Plateau was emplaced onto the now-subducted Farallon Plate, its original volume may have been greater still (Schlanger et al., 1981). Poor resolution of age constraints for both Greater Ontong-Java Plateau volcanism and the start of OAE1a has inhibited determination of whether Greater Ontong-Java Plateau emplacement preceded, was simultaneous with, or post-dated the CIE (e.g. Mahoney et al., 1993; Parkinson et al., 2002; Tejada et al., 2002, 2009). However, a pronounced shift towards non-radiogenic strontium- and osmium-isotope compositions broadly correlative with the basal OAE1a strata in numerous stratigraphic records around the world indicates a large increase in mantle-derived volcanism around the onset of the OAE (e.g. Jones et al., 1994; Bralower et al., 1997; Jones and Jenkyns, 2001; Tejada et al., 2009; Bottini et al., 2012; Martínez-Rodríguez et al., 2021; Percival et al., 2021a), generally attributed to Greater Ontong-Java Plateau activity.

The second Aptian LIP is the High Arctic Large Igneous Province (HALIP), which was emplaced via both subaerial and submarine eruptions and widespread intrusions in pulsed episodes across the Arctic region (Fig. 1; Maher, 2001; Estrada and Henjes-Kunst, 2013; Corfu et al., 2013; Senger et al., 2014; Evenchick et al., 2015; Polteau et al., 2016; Davis et al., 2017; Dockman et al., 2018; Naber et al., 2021; Bédard et al., 2021; Galloway et al., 2022). This emplacement occurred in two major episodes, the first around the middle Hauterivian to early Aptian (spanning c. 127 to 120 Ma of pulsed volcanism, peaking at c. 122 Ma; Evenchick et al., 2015; Dockman et al., 2018; Bédard et al., 2021; Galloway et al., 2022). The later episode(s) took place during the Late Cretaceous (younger than 100 Ma; Dockman et al., 2018 and references therein; Naber et al., 2021; Bédard et al., 2021; Galloway et al., 2022). In the Canadian Arctic Archipelago (Sverdrup Basin), igneous rocks (including mafic lavas and intrusions, and bentonites) are found mainly on Ellef Ringnes, Amund Ringnes, Axel Heiberg and Ellesmere islands (Evenchick et al., 2015; Estrada and Henjes-Kunst, 2013; Davis et al., 2017; Dockman et al., 2018; Evenchick et al., 2019; Naber et al., 2021; Bédard et al., 2021; Galloway et al., 2022). In the Svalbard and Barents Basin, the HALIP is marked by the: (i) intrusion of dolerites as sills into Carboniferous to Jurassic strata on Spitsbergen (Nejbert et al., 2011); (ii) occurrence of bentonites in Cretaceous deltaic sediments on Spitsbergen (Corfu et al., 2013; Midtkandal et al., 2016); (iii) extrusion of lavas on Kong Karls Land (Maher, 2001; Senger et al., 2014); and iv) extensive Cretaceous igneous rocks in the Barents Basin (Polteau et al., 2016). It has been suggested that the first phase of HALIP volcanism is at least partially responsible for triggering OAE1a (Polteau et al., 2016; Galloway et al., 2022), yet, the relative timings between the emplacement of these LIP rocks and OAE1a are not fully understood.

This study sets out to assess the possible influence on and relative timing of eruptive volcanism to the CIE events outlined above, in particular the HALIP, through examining the sedimentary mercury (Hg) record from Arctic localities. Despite a number of caveats and considerations, Hg enrichment in the sedimentary record has been used as a proxy for volcanic eruptions, as volcanism is one of the major natural sources of Hg to the atmosphere (e.g. Sanei et al., 2012; Grasby et al., 2019; Percival et al., 2021b; Edwards et al., 2021). We investigate two sections from the East and West coast of Spitsbergen in the Svalbard archipelago, and two localities from Axel Heiberg Island in the Canadian Arctic, to determine if Hg is elevated across CIEs and contemporaneous with LIP activity in the Arctic. We compare our results to global Hg and $\delta^{13}C$ records, and discuss the possible links between the CIEs and LIP volcanism.

2. Geological setting

Today, the Canadian Arctic and Svalbard Archipelagos lie west and east of Northern Greenland, respectively (Fig. 2). The Svalbard archipelago is part of the greater Barents Sea region, located on the northwestern corner of the Barents Shelf. The largest island, Spitsbergen, has Mesozoic rocks outcropping on the eastern and western flanks of the Central Spitsbergen Basin (Fig. 2C; Johnsen et al., 2001; Dallmann, 1999; Dallmann et al., 2002; Helland-Hansen and Grundvåg, 2021).

Both the Spitsbergen domain and Sverdrup Basin formed part of the circum-Arctic Boreal Realm, which included Northern Alaska and Northern Greenland, and were situated along the northern margins of North America and Eurasia during the Late Jurassic and Early Cretaceous (Fig. 2A; Torsvik et al., 2002). The Boreal Realm saw the formation of numerous rift basins during the Late Jurassic due to the break-up of Pangea (Harland, 1997). Late Cretaceous thermal uplift and early Cenozoic shoulder uplift along the rifted margin of the developing Arctic Ocean, followed by transform movements along the western margin, were responsible for the emergence of the Svalbard Archipelago to its current configuration (Dallmann, 1999). The post-Cretaceous Eurekan Orogeny folded and eroded equivalent strata from Ellesmere Island (Gion et al., 2017), thereby precluding the possibility of acquiring data that might link the two basins.

2.1. Axel Heiberg, Canadian Arctic Archipelago

Sediment deposition in the Canadian Arctic Archipelago in the Late Jurassic and Early Cretaceous occurred during rifting and post-rift

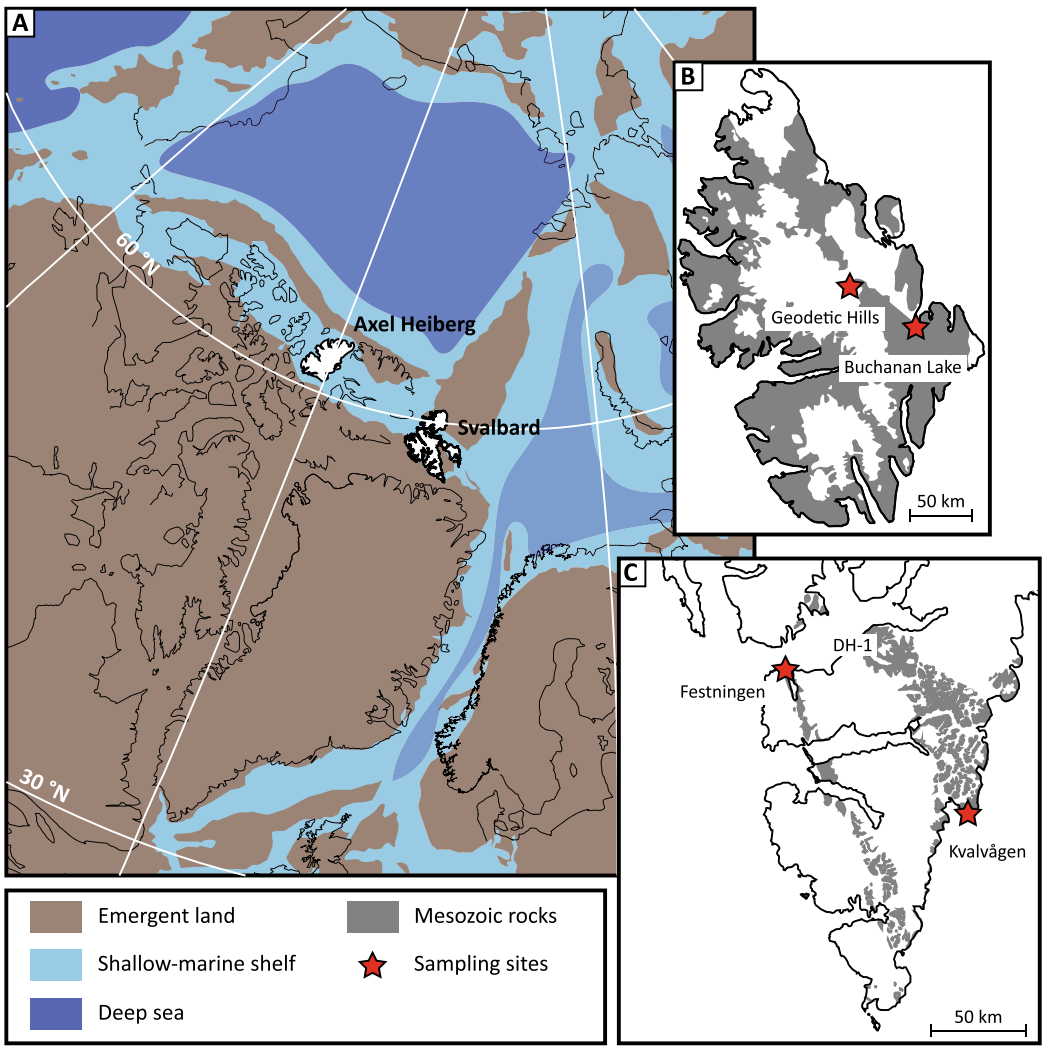

Fig. 2. (A) Palaeogeographic reconstruction for the earliest Cretaceous, c. 140 Ma (after Blakey, 2020; *https://deeptimemaps.com/arctic*). (B) Sampling sites on Axel Heiberg Island. (C) Sampling sites on Spitsbergen.

subsidence of the Sverdrup Basin (Embry and Beauchamp, 2019). Deposition of the Kimmeridgian – Valanginian Deer Bay Formation occurred during peak rifting in the basin (Embry and Beauchamp, 2019). The Deer Bay Formation comprises offshore shelf mudstones, and is undivided except on southern Axel Heiberg Island, where the sandstone-dominated Glacier Fiord Member is identified in its upper part (Embry, 1985). Whilst the Deer Bay Formation is characteristically mudstone-dominated, it has carbonate concretions of variable size and type occurring throughout (Grasby et al., 2017). The top of the Deer Bay Formation is disconformable to conformable with the overlying Hauterivian, Valanginian, or Aptian to Aptian-aged Isachsen Formation (Hadlari et al., 2016; Embry and Beauchamp, 2019; Galloway et al., 2022).

2.2. Spitsbergen, Svalbard Archipelago

During the Late Jurassic and Early Cretaceous, deposition in Spitsbergen occurred in an epicontinental platform and ramp setting (Midtkandal and Nystuen, 2009; Jelby et al., 2020b; Grundvåg et al., 2021), and comprised a range of depositional environments, from offshore shelf through to coastal plain and fluvial environments of the Adventdalen Group (Dypvik et al., 2002; Grundvåg et al., 2019; Midtkandal et al., 2020). This group is sub-divided into the: (i) offshore to prodeltaic mud-, silt- and sandstones of the Bathonian – lower Barremian Janusfjellet Subgroup (e.g. Grundvåg et al., 2019; Jelby et al., 2020a, 2020b); (ii) sandstone-dominated fluvio-deltaic, Barremian – Aptian Helvetiafjellet Formation (e.g. Midtkandal and Nystuen, 2009; Midtkandal et al., 2016); and (iii) shelf–shoreface mud-, silt- and sandstones of the Aptian–Albian Carolinefjellet Formation (e.g. Grundvåg et al., 2021). The Janusfjellet Subgroup is further sub-divided into the Bathonian – Ryazanian Agardhfjellet Formation, deposited in an open-marine environment (Koevoets et al., 2018), and the Valanginian – lower Barremian Rurikfjellet Formation (Śliwińska et al., 2020), which was deposited in an open-marine shelf to prodeltaic setting (Grundvåg et al., 2019; Jelby et al., 2020b). The two formations are transitionally separated by a glauconitic, plastic clay unit termed the Myklegardfjellet Bed (Dypvik et al., 1992), which probably represents the onshore equivalent of the similar-aged base-Cretaceous unconformity recorded in adjacent offshore areas (e.g. Lundin and Dore, 1997). A lower Barremian subaerial unconformity of variable magnitude is observed regionally across Spitsbergen; the result of a prolonged relative sea-level fall that was likely due to the onset of northerly uplift/doming. The fluvio-deltaic deposits of the Helvetiafjellet Formation thus unconformably overlie and erosionally truncate the Rurikfjellet Formation, and grade conformably into the transgressive marine Carolinefjellet Formation of Aptian–Albian age (Mørk et al., 1999).

3. Materials and methods

3.1. Materials

Two sites on Axel Heiberg Island, Geodetic Hills (79°48′N, 89°48′W) and Buchanan Lake (79°22′N, 87°46′W) (Fig. 2B) were targeted for inorganic geochemical analyses, including Hg, and pyrolysis organic chemistry. The lithology and biostratigraphy of these sections are described in Galloway et al. (2020). Both sections span the uppermost Jurassic VOICE event and the Lower Cretaceous Weissert Event CIE, with age control based on macrofossils (ammonites and bivalves) and correlation of bulk organic carbon isotope curves (Galloway et al., 2020). Altogether, 92 samples were collected from Volgian through to Valanginian strata at Geodetic Hills, and 154 samples from the correlative section at Buchanan Lake, with excavation of the surface to 30–50 cm to ensure collection of unweathered samples.

Two sites on Spitsbergen, Festningen (78°05′N, 13°56′E) and Kvalvågen (77°29′N, 18°11′E), were selected for sampling, located on each side of the Central Spitsbergen Basin, where Mesozoic strata are exposed (Fig. 2C). The targeted successions capture the Weissert Event and OAE1a CIEs (Vickers et al., 2019; Jelby et al., 2020a), with the VOICE interval hypothesised to occur somewhere in the 260 m stratigraphically below the yellow-weathering Myklegardfjellet Bed, based on the findings of Jelby et al. (2020a).

The first locality, Festningen, is situated on the western side of Spitsbergen (Fig. 2C), where the entire Adventdalen Group is exposed as vertically bedded coastal cliffs. The exposure is excellent over much of the >600 m succession, with only a few metre- to tens of metre-long gaps where the outcrop was scree-covered/difficult sample, or where the succession is faulted and folded.

On the eastern coast of Spitsbergen, sub-horizontally bedded mid-lower Cretaceous strata (Helvetiafjellet and Carolinefjellet formations) are exposed in the mountains around Kvalvågen (Fig. 2C). These sediments were targeted as they were believed to cover the interval containing the OAE1a (based on the correlation of Grundvåg et al., 2017). Whilst there are excellent outcrops on the vertical eastward-facing cliffs of Kvalhovden, they are generally only accessible along the gentler, scree-covered south and south-western slopes. Thus, sampling was mostly undertaken by digging into the scree in the upper parts of the succession, excavating up to 1 m into the slope to access fresh material. In total, 313 samples were collected from the Volgian through to the Aptian at Festningen, and 39 samples were collected from the Barremian to Aptian part of the succession at Kvalvågen.

Samples from all sites were analysed for Hg concentrations, inorganic elemental concentrations, and sequential pyrolysis. In addition, sedimentological logging and carbon-isotope analysis were undertaken where published information was unavailable. Nine sediment samples were selected for palynological examination from the Kvalvågen section for age control.

3.2. Sequential pyrolysis

The bottom 260 m and top 238 m of the studied part of the Festningen section (84 samples and 96 samples, respectively), and the entire sampled Kvalvågen section (39 samples) were measured using programmed pyrolysis by HAWK at the Lithospheric Organic Carbon Laboratory at Aarhus University, Denmark. Pyrolysis data for the Axel Heiberg localities was also produced using HAWK and are published in Galloway et al. (2020). The quantity and quality of organic carbon was measured using an open, anhydrous, programmed pyrolysis method (Hawk instrument, Wildcat Technologies, USA). The Rock-Eval 6 heating procedure was applied, in which 50 mg of dry, ground sample is subject to a two-step, programmed pyrolysis (heating in an inert atmosphere from 300 to 650 °C) and subsequently oxidation heating (combustion in O_2 atmosphere from 400 to 850 °C) (Lafargue et al., 1998). During the pyrolysis step, the sample is heated to an isotemperature of 300 °C for 3 min to release the free hydrocarbons in the rock (S1, mgHC/g rock). The sample is then subject to a ramped heating from 300 to 650 °C at the rate of 25 °C min-1. The total concentration of the hydrocarbons released due to the thermal cracking kinetics is regarded as S2 (mg HC/g rock), which represent the remaining potential of hydrocarbons in the sample. The organic-derived fractions of CO, and CO_2 released during the ramp heating pyrolysis is the S3 fraction, which represents the content of the oxygen containing organic carbon in the sample. The sum of S2 and S3 is the pyrolysable organic carbon wt% fraction that constitutes "reactive organic carbon" content of the organic matter in a sample. The sample was then automatically transferred to the oxidation oven in which both the residual organic matter and mineral carbon are combusted between 400 and 850 °C. The "residual organic carbon" (RC wt%) is the content of the residual organically-derived CO and CO_2 during the oxidation heating stage. The reactive organic carbon represents the fraction of carbon that is released due to thermal decomposition kinetics of organic matter and hence is considered chemically reactive compared to the refractory "residual organic carbon". The sum of the reactive organic carbon and residual organic carbon is equivalent to TOC wt%. Hydrogen index (HI) is S2/TOC x 100 and is proportional to the H/C ratio. Similarly, oxygen index (OI) is S3/TOC x 100 and is proportional to the O/C ratio. T_{max} is the temperature at which the maximum rate of hydrocarbon generation occurs (peak of S2). Analyses of standard reference material WT1 (developed by the Wildcat Technologies, Houston, U.S.) was run every tenth sample. Duplicate analyses were conducted for assessment of analytical precision. A total of 18 randomly-selected duplicate samples (14 from Festningen and 4 from Kvalvågen) were run for quality control. The results show an accuracy and precision of better than 6% for TOC (see supplementary materials).

Forty samples from the middle of the Festningen section between 29 and 192 m, targeting the Weissert Event CIE interval, were measured by Rock-Eval analysis at the Department of Earth Sciences, University of Oxford, following the protocols of Espitalié et al. (1977) and Behar et al. (2001). Eight measurements of internal standard SAB 134 (calibrated against the certified international standard IFP 160000) were used to monitor machine accuracy and reproducibility, and averaged 2.64 ± 0.02 wt% (1σ), broadly consistent with long-term measurements for the laboratory (2.87 ± 0.11 wt%; Storm et al., 2020).

3.3. Carbon isotope analysis

Carbon isotope data for both Axel Heiberg sections is published in Galloway et al. (2020); and the carbon isotope data for the lower Cretaceous-aged part of the Festningen section is published in Vickers et al. (2016, 2019). Additional carbon-isotope analysis was undertaken for this study on the upper Jurassic succession at Festningen and the Kvalvågen section.

Carbon isotope analysis was undertaken on bulk organic matter, following the decarbonation method of Gröcke et al. (1999). A total of 84 decarbonated samples from the bottom 260 m of the Festningen section were analysed for $\delta^{13}C_{org}$ using an Elemental VarioEL Cube Elemental Analyzer followed by a trap-and-purge separation and online analysis by continuous flow with a DeltaPlus Advantage isotope ratio mass spectrometer coupled with a ConFlo III interface at the GG Hatch Stable Isotope Laboratory, University of Ottawa. Results are reported as ‰ relative to Vienna Pee Dee Belemnite (V-PDB) and normalised against internal standards that are themselves calibrated to the international certified reference materials IAEA-CH-6 (−10.4‰), NBS-22 (−29.91‰), USGS-40 (−26.24‰) and USGS-41 (37.76‰). Long-term analytical precision is based on blind analysis of the internal standard C-55 (glutamine; −28.53‰; not used for calibration), and the mean RPD is 0.20 ± 0.25% SD. In order to assess measurement repeatability, 9 samples were analysed in duplicate.

A total of 40 decarbonated bulk powdered samples from Kvalvågen were analysed using a Sercon Integra gas source isotope ratio mass

spectrometer at the University of Exeter, Penryn Campus. Measurements were performed using decarbonated bulk rock powder with a target weight equivalent to c. 400 μg organic. Instrumental drift was corrected by monitoring of two in-house standards (alanine, $\delta^{13}C_{org} = -19.62$ ‰ and bovine liver, $\delta^{13}C_{org} = -28.61$ ‰) which were previously calibrated against international reference materials and measured after each block of ten samples. A two-point calibration of drift-corrected data from the two in-house standards was taken to correct for instrumental bias and accuracy cross-checked with in-house materials used at the British Geological Survey in Keyworth (SoilA, SoilB, SoilC). Reproducibility of the $\delta^{13}C_{org}$ data relevant for the samples as determined by repeat measurements over three runs from January 2020 to March 2020 is better than 0.2 ‰ (2 s.d.) for both in-house standards (alanine: $n = 44$; bovine liver: $n = 22$).

3.4. Elemental analysis

Inorganic elemental analyses were performed on a regularly-spaced subset of samples for each section (targeting the CIE event intervals), using Inductively Coupled Plasma Mass Spectrometry (ICP-MS) at Bureau Veritas, Vancouver, British Columbia, following four-acid digestion (MA250 package). Briefly, 0.25 g samples were heated in HNO_3, $HClO_4$ and HF to fuming and taken to dryness. The residue was then dissolved in HCl. Analysis for 59 different elements was by ICP-ES/MS, including Mo, Mn, Fe, Sr, Ca, Al and S. A total of 153 samples were analysed from the Buchanan Lake section, 91 samples from the Geodetic Hills section, 119 samples from the Festningen section, and 20 from the Kvalvågen section.

In order to assess measurement repeatability, several samples from each batch were analysed in duplicate. For the Spitsbergen samples, five samples were analysed in duplicate, and for the Axel Heiberg samples, seven samples were analysed in duplicate. Analytical accuracy and precision was monitored through analysis of laboratory standards (STD OREAS45E and STD OREAS25A-4A, $n = 10$ each), 10 blanks, and four preparation blanks (acid wash).

3.5. Mercury analysis

The analysis of Hg concentrations was undertaken at two laboratories. One suite of analyses, on samples spanning the Jurassic–Cretaceous boundary and Barremian–Aptian (investigating the VOICE and OAE1a CIE), was undertaken at the Centre for Earth Observation Science, University of Manitoba, on a Hydra II_C Direct Mercury Analyzer (Teledyne) following the methodology outlined in Sanei et al. (2021). For each sample, between 10 and 50 mg of the homogenized powder was used. Calibration and quality assurance/quality control were carried out by using various certified reference materials (CRMs) including MESS-3 and PACS-3 (marine sediment CRMs from National Research Council of Canada), and NIST 2709a (San Joaquin Soil CRM from NIST). The mean CRM recoveries were 101.9 ± 9.0%.

A second suite of analyses on Valanginian samples from Festningen, which were expected to extend across the Weissert Event interval CIE, was carried out at the Department of Earth Sciences, University of Oxford, using a RA-915 Portable Mercury Analyzer with PYRO PYRO-915 Pyrolyzer (Lumex), following the methodology outlined in Percival et al. (2017). Between 50 and 100 mg samples of rock powder were used, and the instrument was calibrated using six standards of peat (NIMT/UOE/FM/001), with further measurements of the peat standard after every ten measurements, which averaged 174 ± 11 ng/g (1σ, $n = 14$), consistent with its certified value (169 ± 7 ng/g).

3.6. Palynology

Approximately 30 g of sediment from nine regularly-spaced samples throughout the succession at Kvalvågen were taken for preparing palynological slides at the Geological Survey of Denmark and Greenland (GEUS). The details of the maceration method are described in Śliwińska et al. (2020), and includes treatment with hydrochloric and hydrofluoric acids, as well as oxidation with HNO_3. All palynological slides and (if available) organic residues are stored at GEUS. All the slides following the final step of preparation (i.e. filtered using a 30 μm nylon mesh) have been digitalised by Robert Williams at the Norwegian Petroleum Directorate and can be viewed in the Supplementary material.

3.7. Statistical analysis

Spearman's rank correlation coefficient and a *t*-test were used to assess the relationships between variables (Hg, $\delta^{13}C$, elemental and pyrolysis analyses) to determine if Hg or carbon-isotope data are related to other parameters. Spearman's rank is a nonparametric test that indicates the strength of the correlation between the two variables of interest, even if the relationship is monotonic rather than linear. The t-test indicates the probability of this correlation being significant. The divisions used to identify the strength (ρ) and significance (p) of the relationship between the variables of interest are shown in Table 1.

4. Results

4.1. Sequential pyrolysis

Measured TOC data for both sections on Spitsbergen are displayed in Figs. 4 and 5; HI, OI, and T_{max} are shown in Fig. 6. For comparative purposes, pyrolysis data for the Axel Heiberg sections as published in Galloway et al. (2020); and both pyrolysis and Hg data for the DH-1 borehole in central Spitsbergen (Fig. 2C), as published in Midtkandal et al. (2016) and Percival et al., 2021a are also shown. The complete datasets (i.e. containing the other measured variables) are given in the supplementary data. Measured TOC from the Agardhfjellet Formation (VOICE interval and below) from Festningen show a mean TOC of 2.12 wt%; range 0.27–8.18 wt% ($n = 84$; Fig. 4). It is noted that average TOC drops off to 0.86 wt% at the top of the Agardhfjellet Formation, going into the Weissert Event interval, and remains low, with a narrower range (0.78 wt%, range 0.21–2.79 wt%; $n = 40$), throughout the lower Rurikfjellet Formation (Fig. 4). TOC is on average higher and more variable across the OAE1a interval a Festningen ($n = 96$), mean = 1.99 wt%, range = 0.41–11.76 wt%, whilst across the OAE1a interval in the Kvalvågen section ($n = 39$), TOC contents are somewhat more variable, ranging from 0.30 to 10.82 wt% (mean 2.27 wt%).

At Festningen, Spitsbergen, T_{max} values (averaging c. 440 °C) across all CIE intervals indicate that the organic matter is mature (Espitalié et al., 1977) (Fig. 6). At the Kvalvågen site on the East coast of Spitsbergen, average T_{max} values the OAE1a interval are even higher (averaging 472 °C), contrary to findings from other East coast localities which places the Mesozoic sediments from western and central Spitsbergen at lower maturation than those from along the East coast (Olaussen et al.,

Table 1
The divisions used to identify the strength (ρ) and significance (p) of the relationship between the variables of interest.

ρ	0.00 - 0.19	none
	0.20 - 0.39	weak
	0.40 - 0.69	moderate
	0.70 - 0.89	strong
	0.90 - 1.00	v. strong
p	>0.1	none
	0.1 - 0.05	weak
	0.05 - 0.01	strong
	<0.01	v. strong

2022). However, higher maturity of Mesozoic sediments is observed around Edgeøya (i.e. < 70 km from Kvalvågen; Olaussen et al., 2022) due to a large volume of sill intrusions, and it may be that more localised magmatic activity led to steeper geothermal gradients affecting the lower Cretaceous sediments at the Kvalvågen locality.

Hydrogen and oxygen indices cannot be confidently interpreted at the high levels of thermal maturation encountered at Kvalvågen (e.g. Tyson, 1995), whereas at Festningen, a significant proportion of the samples are immature enough to determine the much of the kerogen falls into the Type III (terrestrial OM), with minor marine OM (Fig. 6). This has been confirmed by independent palynofacies, microscopy and biomarker examination of the organic matter indicates that the organic matter present in the Jurassic-Cretaceous strata at Festningen is predominantly terrestrially – derived (Vickers et al., 2019).

4.2. Carbon isotope record

Organic carbon isotope data for the Axel Heiberg sections were presented in Galloway et al. (2020) and have been included for comparative purposes in Fig. 3. Organic carbon isotope data for the Cretaceous succession at Festningen are presented in Vickers et al. (2016, 2019), and are included for comparative purposes in Fig. 4.

Across the uppermost Wilhelmøya Subgroup and Agardhfjellet Formation at Festningen, Spitsbergen (−260 to 0 m; Fig. 4), $\delta^{13}C_{org}$ values range from −31.5 to −22.8 ‰, with a mean of −27.2 ‰. The $\delta^{13}C_{org}$ data are scattered but generally lie around a mean of −25.8 ‰ from −265 m to −106 m (Fig. 4). This is followed by a sharp decline to more negative values that persist for c. 50 m. The $\delta^{13}C_{org}$ values then increase over c. 20 m to −27.0 ‰, in broad agreement with the mean $\delta^{13}C_{org}$ value for the lowermost part of the Rurikfjellet Formation as measured by Vickers et al. (2019) and Jelby et al. (2020a).

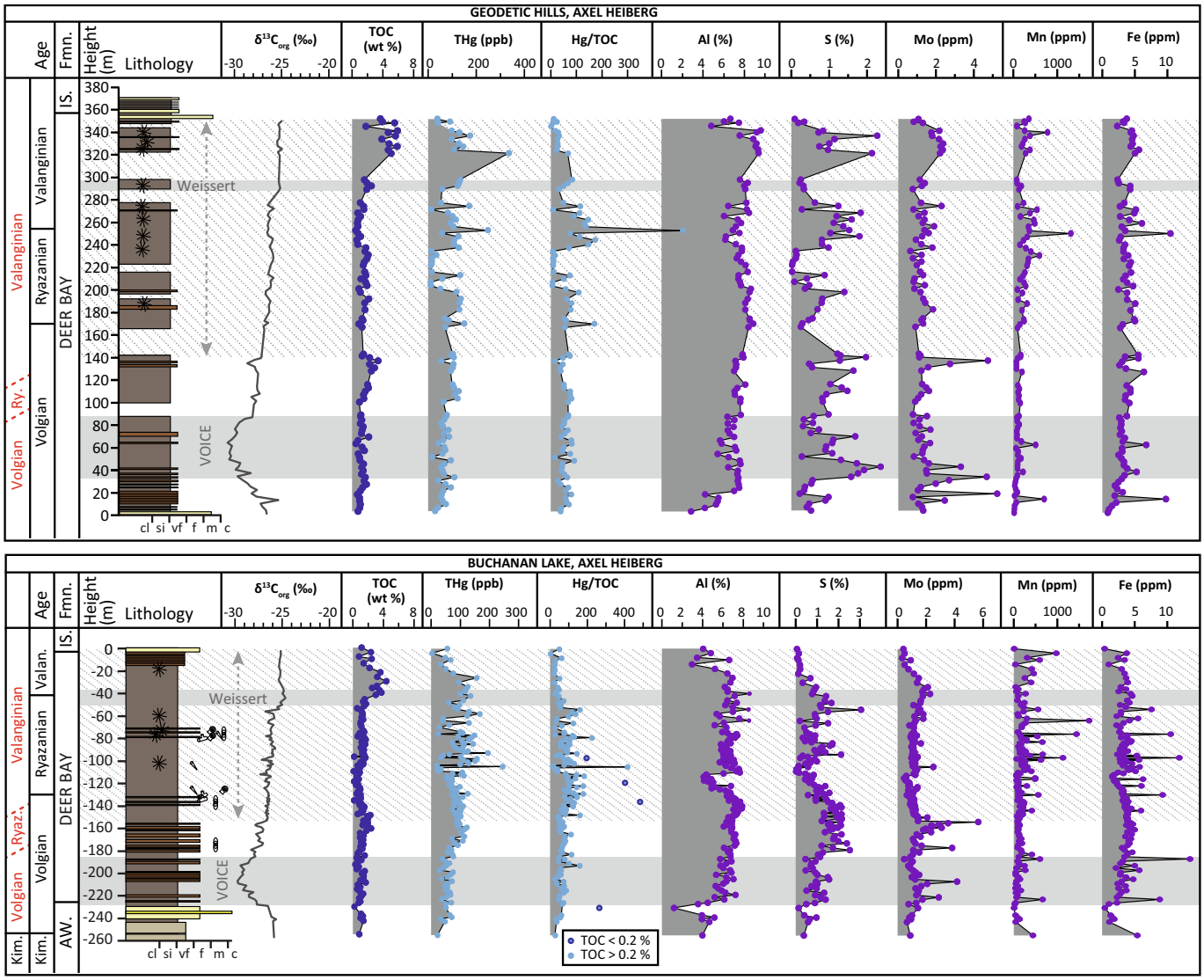

Fig. 3. Organic carbon isotope ratio ($\delta^{13}C_{org}$), total mercury (THg), total organic carbon (TOC), mercury normalised against TOC (Hg/TOC). Where TOC was <0.2% and therefore below the limit for reliability according to Grasby et al. (2016), we denote with dark blue open circles in the Hg/TOC plot, and exclude from subsequent interpretation. Selected elemental data for the two sites on Axel Heiberg, Canadian Arctic, spanning the Jurassic – Cretaceous boundary. Graphic log, carbon isotope and TOC data are all published in Galloway et al. (2020). Other data analysed for this study. The stratigraphic ages are as given in Galloway et al. (2020) based on (limited) biostratigraphic data. New proposed ages based on carbon isotope correlation with Spitsbergen borehole $\delta^{13}C_{org}$ curves from Jelby et al. (2020a). Grey shaded blocks highlight the VOICE interval, and the possible interval for Weissert Event positive CIE (grey shows the Weissert CIE interval as proposed by Galloway et al., 2020, and hatched bands shows the interval as proposed in this study). (For interpretation of the references to colour in this figure legend, the reader is referred to the web version of this article.)

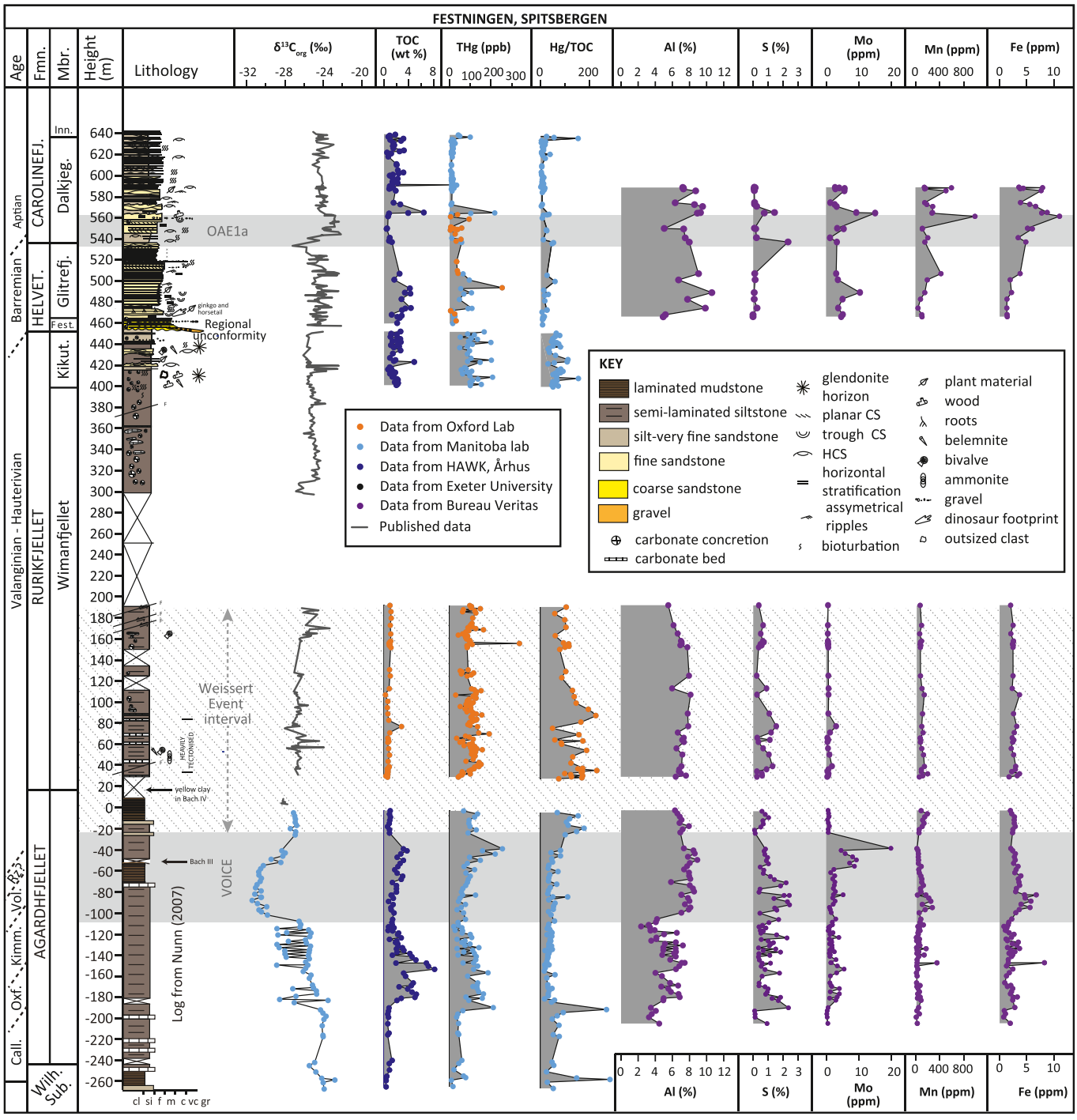

Fig. 4. Organic carbon isotope ratio ($\delta^{13}C_{org}$), total mercury (THg), total organic carbon (TOC), mercury normalised against TOC (Hg/TOC), and selected elemental data for the Festningen section, Spitsbergen, spanning the latest Jurassic and Early Cretaceous. Graphic log, ages, and carbon isotope data shown as a line, are from Vickers et al. (2019). The stratigraphic column for the Agardhfjellet Formation is modified from Nunn (2007). The precise age divisions within the Kimmeridgian to Hauterivian interval is uncertain due again to a lack of biostratigraphically useful fossils, gaps in the carbon isotope record (Vickers et al., 2019), and poor correlation between Boreal and lower latitude (e.g. Tethyan) sites (Gradstein et al., 2020; Jelby et al., 2020a). Grey shaded blocks highlight (from bottom to top) the Volgian carbon isotope excursion ("VOICE" event), and the OAE1a CIE. The proposed interval for Weissert Event positive CIE is denoted by hatched bands.

For the Kvalvågen section on Spitsbergen, the $\delta^{13}C_{org}$ values range from −25.8 to −21.0 ‰, with a mean of −23.7 ‰. The most negative value (−25.8 ‰) is reached at 100 m and is followed by a nearly 5 ‰ increase over three data points to the Least negative value (−21.0 ‰) recorded, at 144 m (Fig. 5).

4.3. Elemental analysis

Elemental analysis was undertaken in order to examine other possible host phases for Hg that may rise from e.g. changes in redox conditions. In both Canadian Arctic sections, and at Festningen, aluminium (which we here use as a proxy for clay), increases sharply at the onset of the VOICE, dropping down slightly at the top of the

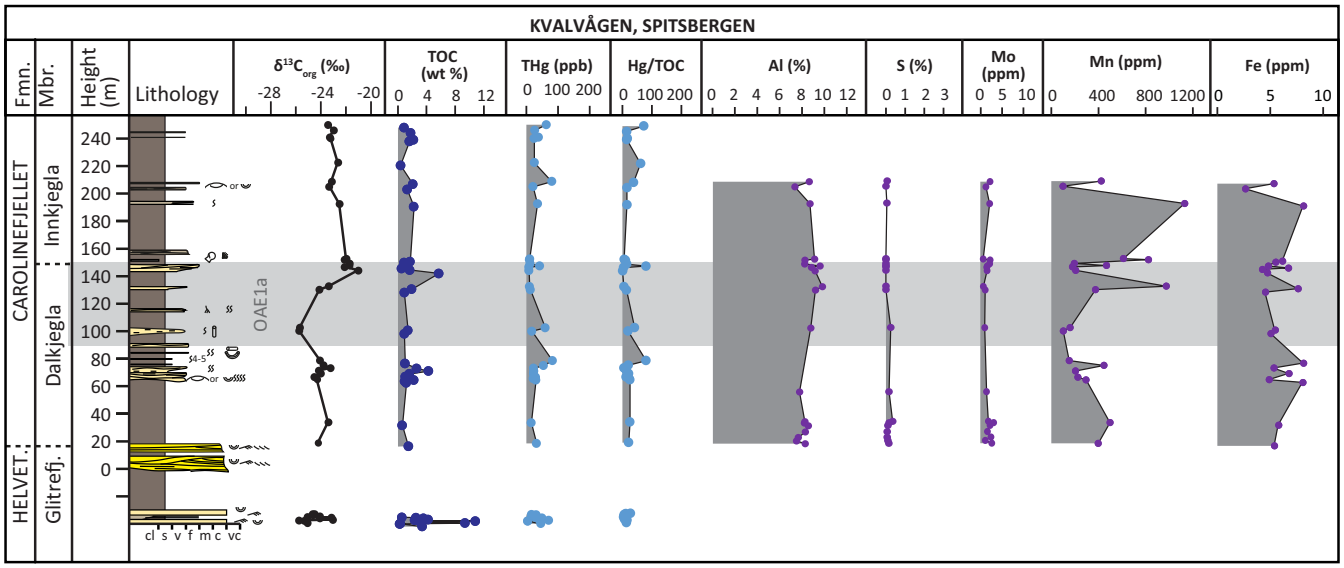

Fig. 5. Organic carbon isotope ratio ($\delta^{13}C_{org}$), total mercury (THg), total organic carbon (TOC), mercury normalised against TOC (Hg/TOC), and selected elemental data across the OAE1a interval for the Kvalvågen section, Spitsbergen.

(possible) Weissert Event interval (Figs. 3 and 4). Aluminium (Al) is more variable across the (proximal, delta front) sediments of the OAE1a interval at Festningen and Kvalvågen (Figs. 4 and 5). Sulphur (S) is variable in the VOICE and Weissert intervals in both Canadian Arctic localities and Festningen (between 0 and 3%; average c. 1%; Figs. 3 and 4). Overall, S is much lower over the OAE1a interval at both Spitsbergen localities, with lowest values in the Kvalvågen section (on average < 0.1%; Fig. 5). Molybdenum (Mo) is on average lower in the Weissert Event interval than the VOICE interval in both Canadian Arctic localities and Festningen (Figs. 3 and 4). At Festningen, Mo is much more variable in the OAE1a interval, and, similar to S, is much lower at Kvalvågen than Festningen (Figs. 4 and 5).

4.4. Mercury record

Measured total mercury concentrations (Hg) are shown in Figs. 3 – 5. Due to variations in TOC content throughout the successions and the known association between Hg and TOC, we discuss the Hg as normalised against TOC (Hg/TOC ratios) (e.g. Sanei et al., 2012; Grasby et al., 2013). Average Hg/TOC across the VOICE interval in the Deer Bay Formation of Axel Heiberg is 72 ppb/wt% for the Buchanan Lake section and 55 ppb/wt% in the Geodetic Hills section, with minimal scatter in the data (Fig. 3). In strata above the VOICE interval, average Hg/TOC values are much higher (100 and 66 ppb/wt% for the Buchanan Lake and Geodetic Hills sections, respectively), with both datasets showing more variability (Fig. 3).

At Festningen (Spitsbergen), the Upper Jurassic Agardhfjellet Formation records Hg of >100 ppb in the Oxfordian – Kimmeridgian strata, which drops to <50 ppb at the base of the VOICE interval before rising to around 250 ppb towards the top of the interval (Fig. 4). This enrichment is matched by similarly elevated TOC contents, resulting in a fairly consistent average Hg/TOC of around 50 ppb/wt% throughout the VOICE interval. Immediately above this CIE, Hg/TOC increases to above 100 ppb/wt% across the uppermost Agardhfjellet – lower Rurikfjellet formations, including the interpreted stratigraphic position of the Weissert Event interval (Fig. 4). Following an interval of poor exposure and no sampling (Fig. 4), the uppermost Rurikfjellet Formation has an average Hg/TOC of 65 ppb/wt% which drops to an average of 15 ppb/wt% across the unconformity at the Rurikfjellet – Helvetiafjellet formation boundary, correlative with a similar decrease in absolute Hg concentrations (from >50 to <30 ppb). This low average Hg/TOC is maintained throughout the Helvetiafjellet and Carolinefjellet formations, with a small peak in the bottom half of the OAE1a interval and the very top of the succession (Fig. 6).

At Kvalvågen (Spitsbergen), Hg/TOC is consistently below 100 ppb/wt% (averaging 21 ppb/wt%) across both Helvetiafjellet and Carolinefjellet formations, but shows a small single-point peak to 81 ppb/wt % just below the OAE1a negative CIE, and reaching lowest values (c. 5 ppb/wt%) coincident with the OAE1a positive $\delta^{13}C_{org}$ shift (Fig. 5).

4.5. Palynology

None of the examined samples from Kvalvågen yielded palynomorphs.

5. Discussion

5.1. Correlations and biases

5.1.1. Carbon isotope trends

In the Festningen section, the negative CIE at −86 m is interpreted to be the VOICE event, as this excursion matches the $\delta^{13}C_{org}$ trends from Hammer et al. (2012), Koevoets et al. (2016), and Jelby et al. (2020a) for other localities across Spitsbergen, as well as the curves from the two Axel Heiberg localities (Galloway et al., 2020). In the Kvalvågen section, the observed excursions at 100 m and 144 m are interpreted to be the OAE1a negative CIE and following positive shift(s) (Fig. 5). The low magnitude of the negative CIE, and single, rather than double positive peak of the OAE1a compared to other $\delta^{13}C_{org}$ records (e.g. Menegatti et al., 1998; Gröcke et al., 1999; Robinson et al., 2008; Herrle et al., 2015) is believed to be due to the relatively sparse sampling. There are no indications that other factors such as OM sourcing play a major role as shown by correlations between $\delta^{13}C_{org}$ and pyrolysis parameters for this locality (Table 2; Fig. 5).

Possible biases in the Upper Jurassic – Lower Cretaceous $\delta^{13}C_{org}$ records from both the Axel Heiberg and Spitsbergen Arctic successions have been assessed by Jelby et al. (2020a), Galloway et al. (2020), and Vickers et al. (2019). These studies found that the trends have not been significantly affected by the thermal maturity of the organic matter, or a change in the proportion of terrestrial vs marine sources. In the new $\delta^{13}C_{org}$ data presented from the VOICE interval at Festningen, Spearman's rank correlation analysis may indicate a weak but significant influence of thermal maturity (as measured by T_{max}) on $\delta^{13}C_{org}$ values ($\rho = 0.31$, $p < 0.005$) (Tables 1 and 2). A negative correlation between HI

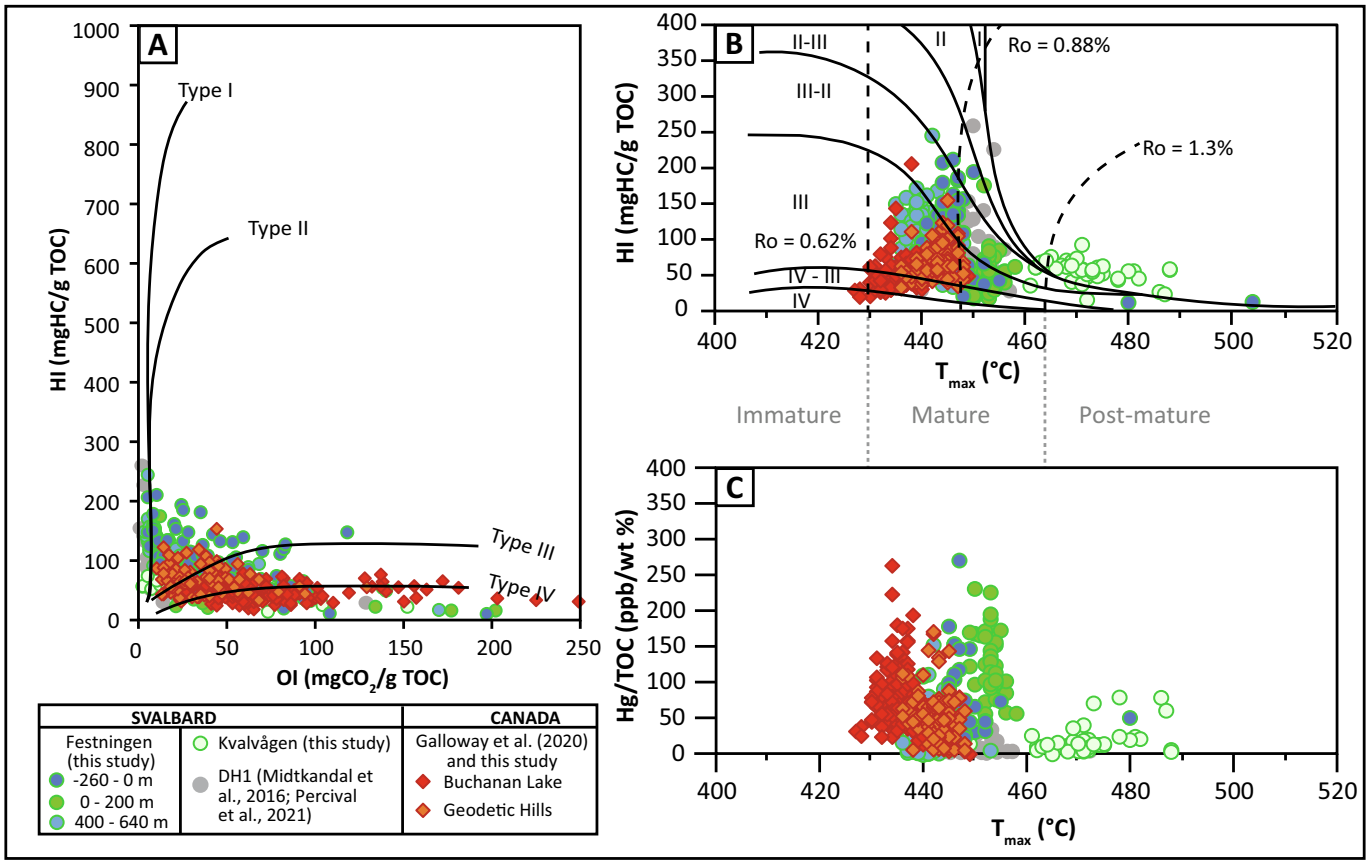

Fig. 6. Selected pyrolysis data. (A) Modified Van Krevelen plot showing OI vs HI as measured for the different intervals (VOICE, Weissert and OAE1a) and localities (Festningen and Kvalvågen on Spitsbergen compared to published data from Buchanan Lake and Geodetic Hills on Axel Heiberg, Galloway et al., 2020), excluding data where TOC was <0.2%. The majority of the samples fall into the fields for Type III kerogen (largely derived from continental plants) and oxidised, inert residual Type IV kerogen, with a smaller fraction falling into the fields for type I (lacustrine-sourced) and II (marine-sourced) kerogen (Tyson, 1995; Hunt, 1996). (B) T_{max} vs HI for the intervals and sections as described for (A), with maturity zones and kerogen types (e.g. organic matter source) indicated. (C) Plot of T_{max} vs Hg/TOC. No correlation is observed between the two variables at any of the sites.

Table 2
Spearman's rank correlations between $\delta^{13}C_{org}$ and measured variables, strength (ρ) and significance (p) for $\delta^{13}C_{org}$ measurements made for this study on Spitsbergen, upper Agardhfjellet and lowest Rurikfjellet formations at Festningen (VOICE interval) and the Kvalvågen section, coloured by strength of the strength and significance of the correlation (as given in Table 1).

$\delta^{13}C$						
Variable	n	ρ Festningen < 0 m	p	n	ρ Kvalvågen	p
S1	84	-0.15	0.172	39	0.16	0.341
S2	84	-0.27	0.011	39	0.12	0.480
S3	84	-0.28	0.009	39	0.31	0.053
T_{max}	84	0.31	0.004	39	0.32	0.051
TOC	84	-0.17	0.133	39	0.09	0.566
HI	84	*-0.49*	*0.000*	39	0.18	0.280
OI	84	0.11	0.331	39	0.00	0.976
OI'	84	0.09	0.400	39	-0.09	0.596

and $\delta^{13}C_{org}$ ($\rho = -0.49$, $p < 0.001$) may highlight biases in the carbon isotope record caused by changes in the source of OM to the sediment. Suan et al. (2015) propose employment of a correction to $\delta^{13}C_{org}$ to remove the effect of amplification of $\delta^{13}C_{org}$ trends by changing organic matter sources. When applied to the Upper Jurassic Festningen data, this correction does not change the magnitude of the VOICE, which remains around 5 ‰ in both uncorrected and corrected $\delta^{13}C_{org}$ values (Fig. 7). Thus, we conclude that the uppermost Jurassic – lowermost Cretaceous negative shifts in $\delta^{13}C_{org}$ in the Festningen section do represent a major disturbance in the Boreal carbon cycle (i.e. likely the VOICE), and is not simply an artefact of variable thermal maturity, or a changing source, of organic matter. In the Kvalvågen section (Helvetiafjellet and Carolinefjellet Formations), no significant correlation is observed between $\delta^{13}C_{org}$ and T_{max}, HI, OI ($\rho < 0.35$, $p > 0.05$; Table 2), indicating that variations in thermal maturity and/or terrestrial vs marine OM have not biased the $\delta^{13}C_{org}$ record at that location (see supplementary data for full suite of analyses).

5.1.2. *Mercury concentrations and normalisation*

Whilst volcanism is generally regarded as a major control on Hg in the geological record, a number of other processes can affect concentrations of this element in sedimentary rocks (see overviews by Sanei et al., 2012, 2015; Grasby et al., 2013, 2019; Percival et al., 2021b). Although Hg is dominantly sequestered with OM in oxygenated marine conditions, Hg may occasionally be removed and buried via other pathways that are partially controlled by ambient redox conditions. Under anoxic-sulfidic conditions, Hg may be bound with sulphide minerals; yet in well-oxygenated settings where both organic matter and pyrite are limited, Hg may be adsorbed onto clay minerals and/or Fe/Mn oxides (e.g. Sanei et al., 2012, 2015; Grasby et al., 2013, 2019). Changes in OM source may affect Hg sequestration in OM (Hammer et al., 2019; Them et al., 2019), as can post depositional processes such as weathering (Charbonnier et al., 2020a). When interpreting the sedimentary

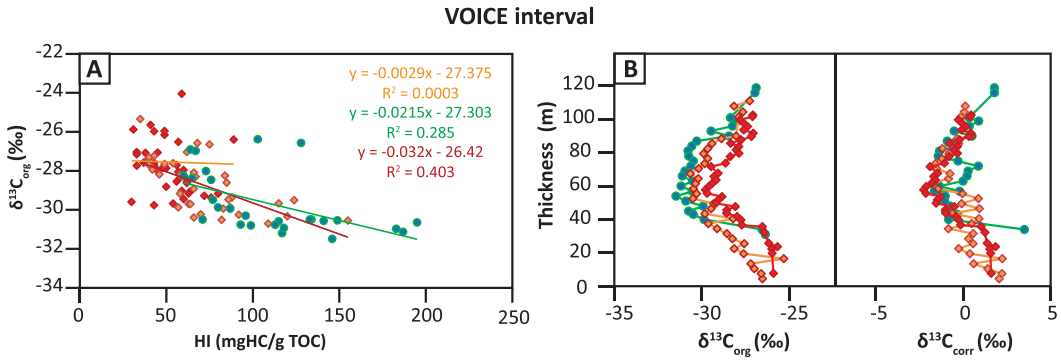

Fig. 7. (A) HI plotted against $\delta^{13}C_{org}$ across the VOICE interval at Buchanan Lake, Geodetic Hills and Festningen, including lines of best fit showing some correlation between the two variables in the Buchanan Lake Geodetic Hills and Festningen samples. (B) Overlaying the VOICE excursion from Buchanan Lake, Geodetic Hills and Festningen before and after application of the Suan et al. (2015) correction for variable organic matter sourcing.

Hg record the influence of Hg sequestration pathways are important to consider as elevated availability of some host-phases (OM, S) can result in higher sedimentary Hg. Previous studies have shown that Hg anomalies, such as those from volcanic activity, can be resolved when normalising to the appropriate sedimentary host-phase (e.g. Grasby et al., 2019). Here, we test whether Hg is associated with organic matter (TOC), sulphur (S), clay minerals (Al) and Mn or Fe oxides.

No single potential Hg carrier is observed to consistently show a strong correlation with Hg across all sites, although Hg is always weakly positively corelated with TOC (Table 3). Aluminium shows a weak correlation with Hg at Buchanan Lake (ρ =0.27; p = 0.001), but not at any of the other studied localities (Table 3); nor do any of the sites show correlation between Hg and Fe, and only the lowest interval at Festningen shows a weak correlation with Mn (ρ = −0.28; p = 0.006). Together, these indicate that adsorption of Hg to clay minerals or Fe/Mn oxides was not significant in these successions.

Sulphur (S) shows weak to moderate correlation in both Canadian arctic localities (ρ = 0.36 at Buchanan Lake and 0.45 at Geodetic Hills, both show $p < 0.001$), suggesting that here, part of the sedimentary Hg is bound with sulphides; yet for the time equivalent interval at Festningen, no correlation between Hg and S is observed (Table 3). The Kvalvågen locality on Spitsbergen also shows a moderate correlation between Hg and S (ρ = 0.66, p = 0.001), which could be consistent with some sulphide-bound Hg at this locality; yet the overall very low concentrations of S at this locality (all <0.4%, on average < 0.1%) suggest that this might be an artefact. High Mo concentrations (>20 ppm) in sedimentary rocks may reflect anoxic conditions (e.g. Tribovillard et al., 2006; Lyons et al., 2009; Hlohowskyj et al., 2021). However, whilst there is a weak correlation between Hg and Mo at both Axel Heiberg sites and the lowest part of the Festningen section (Table 3), the Mo concentrations are consistently low (< 10 ppm excepting one outlier of c. 20 ppm; Figs. 3 and 4) in these parts of the successions, well below that expected during deoxygenation (Tribovillard et al., 2006; Lyons et al., 2009). On Spitsbergen, sedimentological evidence indicates that periodic low-oxygen conditions have affected the Volgian strata, as indicated by the occasional presence of black shales (Koevoets et al., 2016), but the rest of the succession is well-oxygenated and much more proximal (Vickers et al., 2019).

Total organic carbon (TOC), often considered the dominant sedimentary Hg-carrier, is only weakly correlated with Hg in all Arctic localities ($0.2 \leq \rho \geq 0.39$; Table 3), and this is only strongly significant ($p < 0.001$) in the Buchanan Lake section and lowest part of the Festningen section (< 200 m). Changes in organic matter type (e.g. marine vs terrestrial) can affect the sedimentary Hg record (e.g. Hammer et al., 2019; Them et al., 2019), due to higher relative Hg/TOC in terrestrial OM. However, only in the Canadian Arctic localities does Hg show weak to moderate correlation with HI (p = −0.43; ρ < 0.001 at Buchanan Lake; p = 0.29; ρ =0.006 at Geodetic Hills), which may be used as a proxy for OM source (Fig. 6). At Festningen in the VOICE-Weissert interval, there is a moderate negative correlation between Hg and OI. This may reflect some influence from changing OM source, possibly not also observed in the HI signal since the very high maturity of the sediments may have altered the original HI signal (e.g. Tyson, 1995; Hunt, 1996).

In both Canadian Arctic and Spitsbergen localities, the Mesozoic succession is thermally mature to post-mature, as indicated by the high T_{max} of pyrolysis data (T_{max} = c. 440 °C at Festningen, Buchanan Lake and Geodetic Hills; 472 °C at Kvalvågen) (Fig. 6). Increasing maturity has been suggested to potentially bias Hg/TOC ratios towards higher values, due to the preferential removal of organic carbon (Charbonnier et al., 2020a). Whilst there is a strong gradient in maturity of sediments across Spitsbergen, as reflected in the different average T_{max} from Festningen vs Kvalvågen, there is limited stratigraphic variation in thermal

Table 3
Spearman's rank correlations between Hg and measured variables, and Hg/TOC and measured variables, strength (ρ) and significance (p) for the two Axel Heiberg and two Spitsbergen sections, coloured by strength and significance of the correlation (as given in Table 1).

	Hg														
Variable	n	ρ	P	n	ρ	P	n	ρ	P	n	ρ	P	n	ρ	P
	Buchanan Lake			Geodetic Hills			Festningen < 200 m			Festningen >400 m			Kvalvågen		
T_{max}	153	***-0.44***	***0.000***	91	-0.18	0.096	124	**-0.12**	**0.199**	96	0.08	0.457	39	0.21	0.194
TOC	153	**0.35**	**0.000**	91	0.22	0.032	124	**0.39**	**0.000**	96	0.23	0.027	39	0.38	0.018
HI	153	***-0.43***	***0.000***	91	**-0.29**	**0.006**	124	**0.11**	**0.224**	96	0.08	0.426	39	0.16	0.325
OI	153	**-0.21**	**0.009**	91	-0.25	0.018	124	***-0.51***	***0.000***	96	**-0.38**	**0.000**	39	-0.30	0.065
Mo	153	**0.27**	**0.001**	91	**0.36**	**0.000**	99	**0.27**	**0.007**	21	0.41	0.066	20	0.29	0.222
Mn	153	-0.08	0.331	91	0.00	0.992	99	**-0.28**	**0.006**	21	-0.20	0.385	20	-0.08	0.753
Fe	153	0.03	0.716	91	0.11	0.296	99	-0.02	0.853	21	-0.43	0.054	20	0.44	0.054
Al	153	**0.27**	**0.001**	91	0.26	0.014	99	0.09	0.374	21	0.40	0.076	20	-0.20	0.400
S	153	**0.36**	**0.000**	91	***0.45***	***0.000***	99	0.16	0.116	21	0.24	0.294	20	***0.66***	***0.001***

maturity within individual sections. Indeed, neither of the Spitsbergen sites (Festningen or Kvalvågen) show a correlation between Hg and T_{max} ($\rho \leq 0.21$; $p > 0.1$; Table 3). On Axel Heiberg, in the Buchanan Lake section there is a moderate correlation between T_{max} and Hg ($\rho = -0.44$, $p < 0.001$), but no such relationship is observed for samples from Geodetic Hills ($\rho = -0.18$, $p = 0.096$).

The weak correlation between Hg and TOC implies that normalising the Hg to TOC in this case may not remove a major TOC-induced trend as intended. However, anoxia is not believed to have characterised the depositional settings in any localities (e.g. Galloway et al., 2020; Vickers et al., 2019), and there is a lack of correlation with clay mineral elements (Table 3). Further, the successions all contain significant amounts of OM (generally $> > 0.5\%$) and, although weak, all sections show positive correlations between Hg and TOC. This suggests that organic carbon is still expected to be the major host phase for Hg in these sediments. Thus, for the purposes of global comparisons, we present the data normalised to TOC in Fig. 8.

5.2. Early Cretaceous volcanism and carbon cycling in the Boreal Realm

The time interval spanned by this study, latest Jurassic to Early Cretaceous, includes four episodes of large-scale volcanism, the subaerial emplacement of the Paraná-Etendeka Traps and of the High Arctic LIP, and submarine emplacement of the Shatsky Rise and the Greater Ontong-Java Plateau. The emplacement of these LIPs approximately coincides with major perturbations in regional and global carbon isotope records. The Shatsky Rise was emplaced over a shorter time period than the observed Boreal-wide VOICE event, though within the same time interval (Mahoney et al., 2005; Geldmacher et al., 2014). The globally-recognised Weissert Event CIE (late Valanginian – early Hauterivian) occurred at around the same time as the Paraná-Etendeka traps were active (Weissert and Erba, 2004; Duchamp-Alphonse et al., 2007; Martinez et al., 2015; Gomes and Vasconcelos, 2021); and the OAE1a CIE (early Aptian) coincides with both HALIP and the Greater Ontong-Java plateau (Jones et al., 1994; Bralower et al., 1997; Jones and Jenkyns, 2001; Tejada et al., 2009; Bottini et al., 2012; Evenchick et al., 2015; Dockman et al., 2018; Bédard et al., 2021; Martínez-Rodríguez et al., 2021; Percival et al., 2021a; Galloway et al., 2022).

For the Late Jurassic, it is unlikely that such a distal location as the Boreal Realm would record a Hg signature from the submarine volcanism at Shatsky Rise, given that the relatively short residence time of Hg in seawater hinders distribution of the element far from a submarine source (see Bowman et al., 2015 Scaife et al., 2017; Percival et al., 2018, 2021a). Instead, any Hg emitted from Shatsky Rise volcanism would likely be most clear at sites proximal to that LIP. Yet, the dearth of Hg studies from across the Jurassic–Cretaceous boundary interval from such archives (Mahoney et al., 2005; Geldmacher et al., 2014) makes it difficult to interpret the Boreal records in the context of Shatsky Rise eruptions. For the Arctic records examined here, no significant change in Hg or Hg/TOC values into the VOICE event is observed in the Festningen

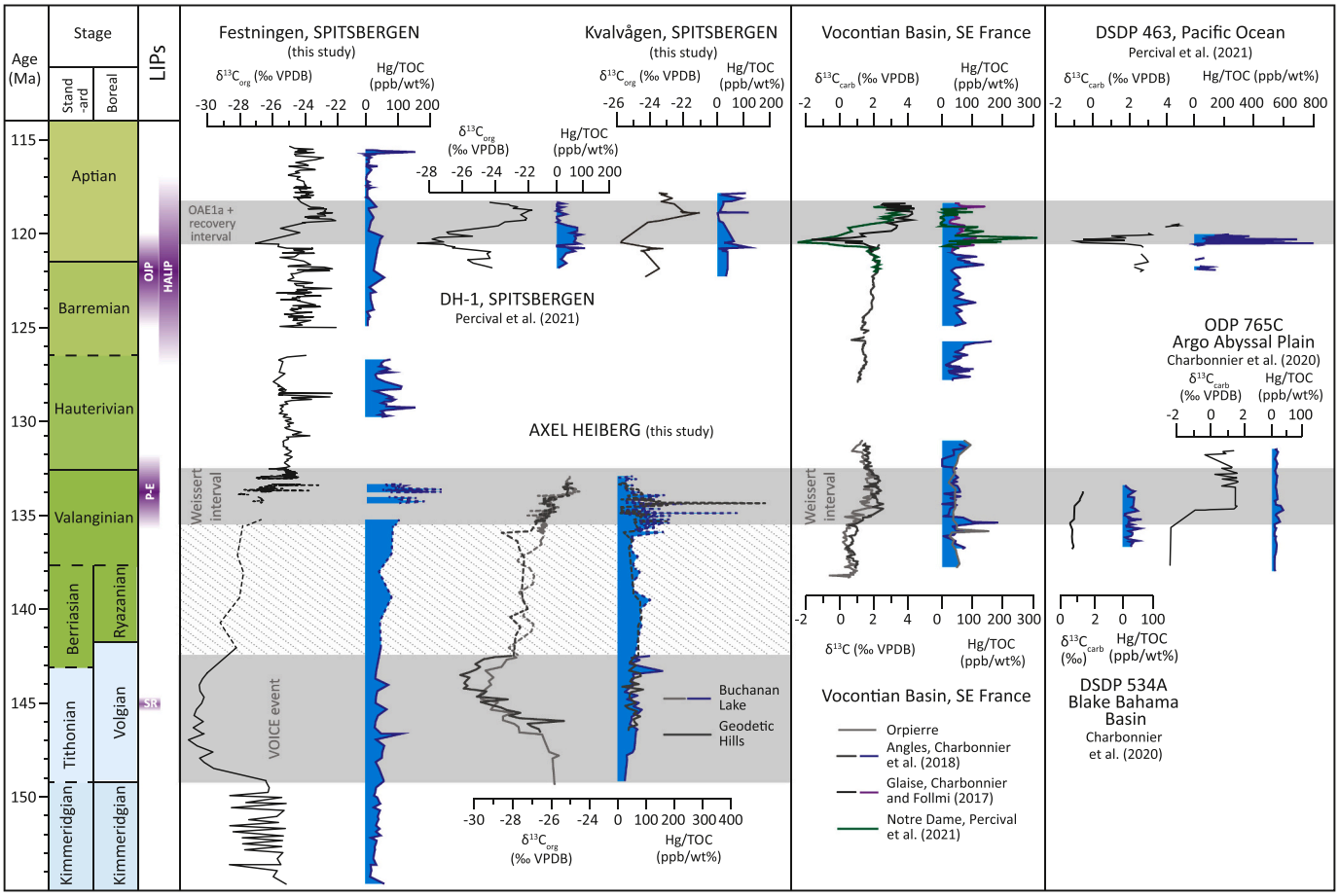

Fig. 8. Comparison of Upper Jurassic to Lower Cretaceous Hg/TOC records (excluding data where TOC was <0.2%) from the Boreal Realm (this study) to those from the Tethyan Realm (Charbonnier et al., 2017; Charbonnier and Föllmi, 2017; Charbonnier et al., 2018), plotted against approximate time (Gradstein et al., 2020). The LIPs ages from Dockman et al. (2018); Gomes and Vasconcelos (2021); Kasbohm et al. (2021); Bédard et al. (2021); and Galloway et al. (2022). Due to the poor biostratigraphic record from the Arctic sections, and uncertainties in the correlation between the Boreal Realm and lower latitudes, the correlation between sites is based on carbon isotope stratigraphy only. The dashed lines indicate the stratigraphic intervals with greatest age uncertainty in the Boreal records, with the cross-hatched interval indicating the possible hiatus in the Arctic records (here not assumed).

section, and fairly constant values are observed throughout the VOICE interval in both Axel Heiberg sections (Figs. 3, 4 and 8). Note that on Axel Heiberg, the record starts too high in the stratigraphy to unquestionably capture the onset of the VOICE (Fig. 3). Our records do not exclude the possibility of distal submarine volcanism playing a causal role, as this may only lead to a local-regional Hg increase (e.g. Percival et al., 2018).

Into the hypothesised Weissert Event interval, all three localities (Buchanan Lake, Geodetic Hills and Festningen) show an increase in Hg and Hg/TOC (Figs. 3 and 4), suggesting a volcanic source for the Hg in this interval. However, detailed interpretation is complicated by the poor age constraints for the studied Arctic sections across the Jurassic-Cretaceous boundary, leading to difficulties locating the Weissert Event CIE in all three sections (Figs. 3 and 4; Galloway et al., 2020; Jelby et al., 2020a, 2020b). Biozone correlations between the Boreal Realm and lower latitudes (e.g. Tethyan Realm) are uncertain due to provincialism and lack of faunal turnover in this interval (e.g. Gradstein et al., 2020). An increase in Hg/TOC is observed in both Spitsbergen and Axel Heiberg localities after the VOICE, which may be synchronous with the start of the Weissert Event positive CIE (Figs. 3 and 4; Jelby et al., 2020a). In the Festningen section, this enrichment occurs across an interval featuring evidence of tectonism, possible hiatuses, and lithological change. In the Axel Heiberg succession, the Weissert Event was previously interpreted as occurring in the upper part of the Deer Bay Formation (Valanginian), based on stratigraphic position above fossils indicative of early Valanginian age in the Buchanan Lake section (Fig. 3; Galloway et al., 2020), and the location of small (< 1 ‰) $\delta^{13}C_{org}$ excursions. Yet, the Weissert CIE is consistently >1.5 ‰ in carbonate ($\delta^{13}C_{carb}$) records (Price et al., 2016 and references therein), and amplified to c. 4–5 ‰ in $\delta^{13}C_{org}$ records (Gröcke et al., 2005; Jelby et al., 2020a). Going by carbon isotope stratigraphic correlation with Spitsbergen of the large excursion (> 3 ‰; Jelby et al., 2020a), the Weissert Event interval may start just after the peak negative of the VOICE (Fig. 3). A linear time-calibrated correlation based on carbon-isotope stratigraphy for the Arctic successions is presented in Fig. 8, yet this must be considered as a best estimate in the absence of stronger age constraints.

The Hg records from lower latitudes do not necessarily show similar trends. In the Vocontian Basin (France; Charbonnier et al., 2017, 2018) Hg/TOC ratios peak sharply just prior to the peak of the Weissert Event, but this peak is of much shorter duration and indeed is only defined by a few data points (Fig. 8). Yet other Tethyan localities show a peak in Hg/TOC at the climbing limb of the Weissert Event (e.g. Polish Basin, Charbonnier et al., 2017; Fig. 8). A recent study of the Hg record across the Argo Abyssal Plain (Indian Ocean; Charbonnier et al., 2020b), shows a similar trend to that seen in the Boreal and Tethyan basins, although it is of much smaller magnitude (Fig. 8). Mercury peaks occur at the onset of the Weissert Event CIE and drop to near zero at the CIE peak (Charbonnier et al., 2020b). Such findings are consistent with increased flux of mercury to the Earth's surface synchronous with the start of the Weissert Event, which may be related to subaerial Paraná-Etendeka volcanism, as recent geochronological studies suggest (e.g. Gomes and Vasconcelos, 2021). However, some of the Paraná-Etendeka volcanics are dated as occurring later (Rocha et al., 2020) or earlier (Dodd et al., 2015) than the onset of the Weissert Event. Consequently, further work is needed to resolve uncertainties in the timescales of both the Paraná-Etendeka volcanism and Valanginian stratigraphic record (particularly outside of the Tethys) in order to confirm the link between these two phenomena (Gradstein et al., 2020).

The OAE1a CIE is unequivocally expressed in the organic carbon record at multiple localities across Spitsbergen (Fig. 8; Vickers et al., 2016, 2019; Midtkandal et al., 2016), and it is also recorded in the Canadian Arctic (Herrle et al., 2015; Dummann et al., 2021). As previously mentioned, this CIE is associated with the emplacement of two LIPs – the largely subaerial and intrusive HALIP (Dockman et al., 2018; Galloway et al., 2022) and the submarine Greater Ontong-Java plateau (Kasbohm et al., 2021) (Figs. 1and8). Any volcanically-driven Hg perturbations observed in the Boreal Realm would be expected to arise from the nearby HALIP rather than the distal, submarine Greater Ontong-Java Plateau (Fig. 1; Percival et al., 2021a).

In the three Spitsbergen sections measured (Festningen and Kvalvågen, this study; and the DH-1 borehole, Percival et al., 2021a), Hg/TOC is slightly raised at the onset of the OAE1a CIE, although the shape of the Hg/TOC curves varies between these sites, and the Hg/TOC spike is much clearer in the DH-1 borehole record (Percival et al., 2021a) than in the two sites presented here. This may be due, in part, to differential thermal overprinting, and partial Hg sequestration into S at the Kvalvågen locality (See section 5.1.2).

The variability in Hg/TOC records from across the globe lead Percival et al., 2021a to conclude that the Greater Ontong-Java Plateau was most likely the dominating LIP at the onset of OAE1a, and that the smaller disturbances in the Boreal and Tethyan records may have been linked to pulses of HALIP volcanism. Since both HALIP and Greater Ontong-Java Plateau volcanism are dated radiometrically as having peaked simultaneously at around 122 Ma (Dockman et al., 2018; Kasbohm et al., 2021), it would be expected that Hg/TOC records from both the Boreal Realm and Pacific might show correlative peaks. However, a spore spike is documented in a succession of Isachsen Formation exposed at Glacier Fiord immediately prior to OAE1a is believed to be related to landscape disturbance associated with extrusive volcanism of the HALIP and interpreted to occur in the latest Barremian, indicating HALIP activity prior to OAE1a (Galloway et al., 2022). The peak in Hg/TOC observed prior to the negative peak of the OAE1a in the DH-1 borehole and Kvalvågen records from Spitsbergen supports this finding. The raised Hg/TOC across the negative peak of the CIE in all three Spitsbergen localities is consistent with continued HALIP activity coincident with the OAE1a (and Greater Ontong-Java Plateau volcanism) (Fig. 8).

6. Conclusions

This study set out to examine the Boreal Realm sedimentary Hg record across three carbon isotope excursions (CIEs) in the Upper Jurassic and Lower Cretaceous, from modern-day Arctic localities, in order to assess the possible link between the CIEs and particular large-scale volcanic events. Parts of the records show some correlation with elemental and sequential pyrolysis parameters, indicating some influence from changing redox conditions and carbon sources across the Jurassic-Cretaceous boundary interval. Nevertheless, we can still interpret the following: 1) The Upper Jurassic – lowermost Cretaceous Volgian Isotopic Carbon Excursion (VOICE) is not associated with any significant perturbations in the Hg records in either the Axel Heiberg or Spitsbergen records, suggesting that the VOICE did not result from localised Arctic volcanic eruptions. However, these data do not discount the possibility of distal submarine volcanism, such as the emplacement of the Shatsky Rise. 2) There are elevated Hg and Hg/TOC ratios correlative with the proposed stratigraphic position of the Weissert Event CIE in both Axel Heiberg and Spitsbergen, which may have been sourced from the Paraná-Etendeka subaerial volcanism. Yet, this increase in Hg is also correlative with a change in lithology and a possible hiatus on Spitsbergen, leaving other possible explanations for the Hg increase, particularly given the potential uncertainties in the stratigraphic model. 3) Two of the three Hg records from Spitsbergen across OAE1a show increased Hg/TOC just prior onset of the OAE1a CIE. This is consistent with recent work which suggests that HALIP activity began in the Late Barremian, preceding that of the Greater Ontong-Java Plateau. The shapes of the Hg/TOC curves across this interval vary spatially across Spitsbergen, and this is believed to be due to a combination of factors, such as variable proximity and perhaps thermal maturity. The much higher thermal maturity at the Kvalvågen site compared to the other localities may have partially overprinted the Hg/TOC at this locality.

Declaration of Competing Interest

The authors declare that they have no known competing financial interests or personal relationships that could have appeared to influence the work reported in this paper.

Data availability

I have shared the data as excel files in the Attach Files stage.

Acknowledgements

Funding for fieldwork for this study was provided by a Ph.D. scholarship from the University of Plymouth, U.K. with additional funding to MLV for field campaigns to sample the Lower Cretaceous of Festningen from the Geological Society, London, UK (Gloyne Outdoor Geological Research fund, 2014); to MLV, MEJ and IM from the National Geographic Society's Committee for Research and Exploration grant number CP-038R-17; and to MLV from The British Sedimentological Research Group Gill Harwood Memorial Fund (2015), and an American Association of Petroleum Geologists grant-in-aid (William E. Gipson Named Grant, 2015). We kindly thank Trude Hohle for invaluable field assistance for MLV, MEJ and KKS in the 2018 campaign at Kvalvågen, Spitsbergen, and Dr. Meriel FitzPatrick for field assistance during the 2014 field campaign. Field work to collect samples from the uppermost Jurassic-lowermost Cretaceous portion of the Festningen section was supported by Bundesanstalt für Geowissenschaften und Rohstoffe (BGR) [Federal Institute for Geosciences and Natural Resources] under the Circum-Arctic Structural Events (CASE) program in 2015 (lead Dr. Karsten Piepjohn). Collections were made by JMG with assistance from SG and LR. Canadian field work was supported by the GeoMapping for Energy and Minerals (GEM) Program (Natural Resources Canada, Geological Survey of Canada) with funding to JMG. Collections were made by JMG with support from Dr. Lisa Neville (GSC Calgary), Kyle Sulphur (GSC Calgary), and Pilipoosie Iqaluk (Hamlet of Resolute Bay, NU) in 2015. Dr. Keith Dewing is thanked for HALIP project activity management. Logsitics support for this work was provided by the Polar Continental Shelf Program (NRCan) and UHL Helicopters (Pilot Lorne Pike). We are grateful for the staff of the Environment and Climate Change Canada Eureka Weather Station and, in particular, Station Manager André Beauchard, where the work was staged from. Mercury, elemental, and sequential pyrolysis of the samples from the uppermost Jurassic-lowermost Cretaceous portions of the Festningen section were funded by a AIAS-COFUND II fellowship programme supported by the Marie Skłodowska-Curie actions under the European Commission's Horizon 2020 (grant agreement no. 754513) and the Aarhus University Research Foundation to JMG (2019-2020). This grant also financially supported Hg analysis of the Kvalvågen section. Data cited from Galloway et al., 2020 are acknowledged therein. Funding was also provided for this study by the European Commission, Horizon 2020 (ICECAP; grant no. 101024218, to MLV), and from the Research Council of Norway through the Centres of Excellence funding scheme, project number 223272. Further funding was provided by the Danish Council for Independent Research–Natural Sciences (project DFF-7014-00142), to CK.; the Canada Research Chairs program to FW. Mercury analyses at the University of Oxford were supported by the Leverhulme Trust and Natural Environment Research Council Grant NE/G01700X/1 and ERC consolidator Grant (ERC-2018-COG-818717-V-ECHO) (to TAM) and PhD studentship NE/L501530/1 (to LMEP), with geochemical standard material provided by John Farmer and the University of Edinburgh. We thank Andrew Kingston for an internal GSC review. This contribution represents NRCan contribution number / Numéro de contribution de RNCan: 20220228. We would like to thank Kim Senger and one anonymous reviewer for their constructive feedback.

Appendix A. Supplementary data

Supplementary data to this article can be found online at https://doi.org/10.1016/j.palaeo.2023.111412.

References

Ando, A., Kakegawa, T., Takashima, R., Saito, T., 2002. New perspective on Aptian carbon isotope stratigraphy: data from δ13C records of terrestrial organic matter. Geology 30 (3), 227–230.
Bédard, J.H., Saumur, B.M., Tegner, C., Troll, V.R., Deegan, F.M., Evenchick, C.A., Grasby, S.E., Dewing, K., 2021. Geochemical systematics of High Arctic large Igneous Province continental tholeiites from Canada—Evidence for progressive crustal contamination in the plumbing system. J. Petrol. 62 (9), p.egab041.
Behar, F., Beaumont, V., Penteado, H.D.B., 2001. Rock-Eval 6 technology: performances and developments. Oil Gas Sci. Technol. 56 (2), 111–134.
Blakey, R., 2020. Deep Time Maps. Inc.TM. https://deeptimemaps.com.
Bodin, S., Meissner, P., Janssen, N.M., Steuber, T., Mutterlose, J., 2015. Large igneous provinces and organic carbon burial: Controls on global temperature and continental weathering during the early cretaceous. Glob. Planet. Chang. 133, 238–253.
Bond, D.P., Grasby, S.E., 2017. On the causes of mass extinctions. Palaeogeogr. Palaeoclimatol. Palaeoecol. 478, 3–29.
Bottini, C., Cohen, A.S., Erba, E., Jenkyns, H.C., Coe, A.L., 2012. Osmium-isotope evidence for volcanism, weathering, and ocean mixing during the early Aptian OAE 1a. Geology 40 (7), 583–586.
Bowman, K.L., Hammerschmidt, C.R., Lamborg, C.H., Swarr, G., 2015. Mercury in the North Atlantic Ocean: the U.S. GEOTRACERS zonal and meridional sections. Deep Sea Res. II 116, 251–261.
Bralower, T.J., Arthur, M.A., Leckie, R.M., Sliter, W.V., Allard, D.J., Schlanger, S.O., 1994. Timing and paleoceanography of oceanic dysoxia/anoxia in the late Barremian to early Aptian (Early Cretaceous). Palaios 9 (4), 335–369.
Bralower, T.J., Fullagar, P.D., Paull, C.K., Dwyer, G.S., Leckie, R.M., 1997. Mid-cretaceous strontium-isotope stratigraphy of deep-sea sections. Geol. Soc. Am. Bull. 109 (11), 1421–1442.
Cavalheiro, L., Wagner, T., Steinig, S., Bottini, C., Dummann, W., Esegbue, O., Gambacorta, G., Giraldo-Gómez, V., Farnsworth, A., Flögel, S., Hofmann, P., 2021. Impact of global cooling on Early Cretaceous high pCO2 world during the Weissert Event. Nature communications 12 (1), 1–11.
Chambers, L.M., Pringle, M.S., Fitton, J.G., 2004. Phreatomagmatic eruptions on the Ontong Java Plateau: an Aptian 40Ar/39Ar age for volcaniclastic rocks at ODP Site 1184. Geol. Soc. Lond., Spec. Publ. 229 (1), 325–331. https://doi.org/10.1144/GSL.SP.2004.229.01.1.
Charbonnier, G., Adatte, T., Föllmi, K.B., Suan, G., 2020a. Effect of intense weathering and postdepositional degradation of organic matter on Hg/TOC proxy in organic-rich sediments and its implicationsfor deep-time investigations. Geochem. Geophys. Geosyst. 21 (2), e2019GC008707.
Charbonnier, G., Adatte, T., Duchamp-Alphonse, S., Spangenberg, J.E., Föllmi, K.B., 2020b. Global mercury enrichment in Valanginian sediments supports a volcanic trigger for the Weissert episode. In: Mass Extinctions, Volcanism, and Impacts: New Developments, 544, p. 85.
Charbonnier, G., Föllmi, K.B., 2017. Mercury enrichments in lower Aptian sediments support the link between Ontong Java large igneous province activity and oceanic anoxic episode 1a. Geology 45 (1), 63–66.
Charbonnier, G., Morales, C., Duchamp-Alphonse, S., Westermann, S., Adatte, T., Föllmi, K.B., 2017. Mercury enrichment indicates volcanic triggering of Valanginian environmental change. Sci. Rep. 7 (1), 1–6.
Charbonnier, G., Godet, A., Bodin, S., Adatte, T., Föllmi, K.B., 2018. Mercury anomalies, volcanic pulses, and drowning episodes along the northern Tethyan margin during the latest Hauterivian-earliest Aptian. Palaeogeogr. Palaeoclimatol. Palaeoecol. 505, 337–350.
Coffin, M.F., Eldholm, O., 1994. Large igneous provinces: crustal structure, dimensions, and external consequences. Rev. Geophys. 32 (1), 1–36.
Corfu, F., Polteau, S., Planke, S., Faleide, J.I., Svensen, H., Zayoncheck, A., Stolbov, N., 2013. U-Pb geochronology of cretaceous magmatism on Svalbard and Franz Josef Land, Barents Sea large Igneous Province. Geol. Mag. 150 (06), 1127–1135.
Courtillot, V., Renne, P.R., 2003. On the ages of flood basalt events. C. R. Géosci. 335, 113–140. https://doi.org/10.1016/S1631-0713(03)00006-3.
Dallmann, W.K., Ohta, Y., Elvevold, S., Blomeier, D., 2002. Bedrock map of Svalbard and Jan Mayen 1:750,000, with insert maps 1:250,000. Norwegian Polar Institute.
Dallmann, W.K., 1999. 1. Introduction. In: Dallmann, W.K. (Ed.), Lithostratigraphic Lexicon of Svalbard, Upper Palaeozoic to Quaternary Bedrock: Review and Recommendations for Nomenclature Use. Norwegian Polar Institute, Tromsø.
Davis, W.J., Schroeder-Adams, C.J., Galloway, J.M., Herrle, J.O., Pugh, A.T., 2017. U-Pb geochronology of bentonites from the Upper cretaceous Kanguk Formation, Sverdrup Basin, Arctic Canada: constraints on sedimentation rates, biostratigraphic correlations and the late magmatic history of the High Arctic large Igneous Province. Geol. Mag. 154 (4), 757–776.
Dockman, D.M., Pearson, D.G., Heaman, L.M., Gibson, S.A., Sarkar, C., 2018. Timing and origin of magmatism in the Sverdrup Basin, Northern Canada—Implications for lithospheric evolution in the High Arctic large Igneous Province (HALIP). Tectonophysics 742, 50–65.
Dodd, S.C., Mac Niocaill, C., Muxworthy, A.R., 2015. Long duration (> 4 Ma) and steady-state volcanic activity in the early cretaceous Paraná-Etendeka large Igneous

Province: new palaeomagnetic data from Namibia. Earth Planet. Sci. Lett. 414, 16–29.
Duchamp-Alphonse, S., Gardin, S., Fiet, N., Bartolini, A., Blamart, D., Pagel, M., 2007. Fertilization of the northwestern Tethys (Vocontian basin, SE France) during the Valanginian carbon isotope perturbation: evidence from calcareous nannofossils and trace element data. Palaeogeogr. Palaeoclimatol. Palaeoecol. 243 (1), 132–151.
Dummann, W., Schröder-Adams, C., Hofmann, P., Rethemeyer, J., Herrle, J.O., 2021. Carbon isotope and sequence stratigraphy of the upper Isachsen Formation on Axel Heiberg Island (Nunavut, Canada): High Arctic expression of oceanic anoxic event 1a in a deltaic environment. Geosphere 17 (2), 501–519.
Dypvik, H., Nagy, J., Krinsley, D., 1992. Origin of the Myklegardfjellet Bed, a basal cretaceous marker on Spitsbergen. Polar Res. 11, 21–31.
Dypvik, H., Håkansson, E., Heinberg, C., 2002. Jurassic and cretaceous palaeogeography and stratigraphic comparisons in the North Greenland-Svalbard region. Polar Res. 21 (1), 91–108.
Edwards, B.A., Kushner, D.S., Outridge, P.M., Wang, F., 2021. Fifty years of volcanic mercury emission research: knowledge gaps and future directions. Sci. Total Environ. 757, 143800.
Embry, A.F., Beauchamp, B., 2019. Chapter 14 Sverdrup Basin. In: Miall, A. (Ed.), The Sedimentary Basins of the United States and Canada, 2nd edition. Elsevier, Amsterdam, pp. 559–592.
Embry, A.F., 1985. In: New stratigraphic units, Middle Jurassic to lowermost Cretaceous succession, Arctic Islands, pp. 269–276. Geological Survey of Canada Current Research Paper 85-1b.
Erba, E., Channell, J.E., Claps, M., Jones, C., Larson, R., Opdyke, B., Premoli Silva, I., Riva, A., Salvini, G., Torricelli, S., 1999. Integrated stratigraphy of the Cismon Apticore (southern Alps, Italy); a "reference section" for the Barremian-Aptian interval at low latitudes. J. Foramin. Res. 29 (4), 371–391.
Erba, E., Bartolini, A., Larson, R.L., 2004. Valanginian Weissert oceanic anoxic event. Geology 32 (2), 149–152.
Erba, E., Duncan, R.A., Bottini, C., Tiraboschi, D., Weissert, H., Jenkyns, H.C., Malinverno, A., 2015. Environmental consequences of Ontong Java Plateau and Kerquelen Plateau volcanism. In: Neal, C.R., Sager, W.W., Sano, T., Erba, E. (Eds.), The Origin, Evolution, and Environmental Consequences of Oceanic Large Igneous Provinces, 511, pp. 271–303. Geol. Soc. Am. Spec. Paper.
Espitalié, J., Madec, M., Tissot, B., Mennig, J.J., Leplat, P., 1977. Source rock characterization method for petroleum exploration. In: Offshore Technology Conference, Houston, Texas. OTC-2935-MS.
Ernst, R.E., 2014. Large igneous provinces. Cambridge University Press.
Estrada, S., Henjes-Kunst, F., 2013. 40Ar-39Ar and U-Pb dating of cretaceous continental rift-related magmatism on the Northeast Canadian Arctic margin. Z. Dtsch. Ges. Geowiss. 164 (1), 107–130.
Evenchick, C.A., Davis, W.J., Bédard, J.H., Hayward, N., Friedman, R.M., 2015. Evidence for protracted High Arctic large igneous province magmatism in the Central Sverdrup Basin from stratigraphy, geochronology, and paleodepths of saucer-shaped sills. GSA Bull. 127 (9–10), 1366–1390.
Evenchick, C.A., Galloway, J.M., Saumur, B.M., Davis, W.J., 2019. A revised stratigraphic framework for cretaceous sedimentary and igneous rocks at Mokka Fiord, Axel Heiberg Island, Nunavut, with implications for the cretaceous Normal Superchron. Can. J. Earth Sci. 56 (2), 158–174.
Galloway, J.M., Fensome, R.A., Swindles, G.T., Hadlari, T., Fath, J., Schröder-Adams, C., Herrle, J.O., Pugh, A., 2022. Exploring the role of High Arctic large Igneous Province volcanism on early cretaceous Arctic forests. Cretac. Res. 129, 105022.
Galloway, J.M., Vickers, M.L., Price, G.D., Poulton, T., Grasby, S.E., Hadlari, T., Beauchamp, B., Sulphur, K., 2020. Finding the VOICE: organic carbon isotope chemostratigraphy of late Jurassic-early cretaceous Arctic Canada. Geol. Mag. 157 (10), 1643–1657.
Ganino, C., Arndt, N.T., 2009. Climate changes caused by degassing of sediments during the emplacement of large igneous provinces. Geology 37 (4), 323–326.
Geldmacher, J., van den Bogaard, P., Heydolph, K., Hoernle, K., 2014. The age of earth's largest volcano: Tamu Massif on Shatsky rise (northwest Pacific Ocean). Int. J. Earth Sci. 103 (8), 2351–2357.
Gion, A.M., Williams, S.E., Mueller, R.D., 2017. A reconstruction of the Eurekan Orogeny incorporating deformation constraints. Tectonics 36 (2), 304–320. https://doi.org/10.1002/2015TC004094.
Gladczenko, T.P., Coffin, M.F., Eldholm, O., 1997. Crustal structure of the Ontong Java Plateau: modeling of new gravity and existing seismic data. J. Geophys. Res. Solid Earth 102 (B10), 22711–22729.
Gomes, A.S., Vasconcelos, P.M., 2021. Geochronology of the Paraná-Etendeka large igneous province. Earth Sci. Rev. 220, 103716.
Gradstein, F.M., Ogg, J.G., Schmitz, M.D., Ogg, G.M. (Eds.), 2020. Geologic Time Scale 2020. Elsevier.
Grasby, S.E., Sanei, H., Beauchamp, B., Chen, Z., 2013. Mercury deposition through the Permo-Triassic Biotic Crisis. Chem. Geol. 351, 209–216.
Grasby, S.E., Beauchamp, B., Bond, D.P., Wignall, P.B., Sanei, H., 2016. Mercury anomalies associated with three extinction events (Capitanian crisis, latest Permian extinction and the Smithian/Spathian extinction) in NW Pangea. Geological magazine 153 (2), 285–297.
Grasby, S.E., McCune, G.E., Beauchamp, B., Galloway, J.M., 2017. Lower cretaceous cold snaps led to widespread glendonite occurrences in the Sverdrup Basin. Can. High Arctic Bull. 129 (7–8), 771–787.
Grasby, S.E., Them II, T.R., Chen, Z., Yin, R., Ardakani, O.H., 2019. Mercury as a proxy for volcanic emissions in the geologic record. Earth Sci. Rev. 196, 102880.
Gréselle, B., Pittet, B., Mattioli, E., Joachimski, M., Barbarin, N., Riquier, L., Reboulet, S., Pucéat, E., 2011. The Valanginian isotope event: a complex suite of palaeoenvironmental perturbations. Palaeogeogr. Palaeoclimatol. Palaeoecol. 306 (1–2), 41–57.
Gröcke, D.R., Price, G.D., Robinson, S.A., Baraboshkin, E.Y., Mutterlose, J., Ruffell, A.H., 2005. The Upper Valanginian (Early Cretaceous) positive carbon–isotope event recorded in terrestrial plants. Earth Planet. Sci. Lett. 240 (2), 495–509.
Gröcke, D.R., Hesselbo, S.P., Jenkyns, H.C., 1999. Carbon-isotope composition of lower cretaceous fossil wood: Ocean-atmosphere chemistry and relation to sea-level change. Geology 27 (2), 155–158.
Grundvåg, S.A., Marin, D., Kairanov, B., Śliwińska, K.K., Nøhr-Hansen, H., Jelby, M.E., Escalona, A., Olaussen, S., 2017. The lower cretaceous succession of the northwestern Barents Shelf: Onshore and offshore correlations. Mar. Pet. Geol. 86, 834–857.
Grundvåg, S.-A., Jelby, M.E., Śliwińska, K.K., Nøhr-Hansen, H., Aadland, T., Sandvik, S. E., Tennvassås, I., Engen, T., Olaussen, S., 2019. Sedimentology and palynology of the lower cretaceous succession of Central Spitsbergen: integration of subsurface and outcrop data. Nor. J. Geol. 99, 253–284.
Grundvåg, S.-A., Jelby, M.E., Olaussen, S., Śliwińska, K.K., 2021. The role of shelf morphology on storm-bed variability and stratigraphic architecture, lower cretaceous, Svalbard. Sedimentology 68, 196–237.
Hadlari, T., Midwinter, D., Galloway, J.M., Durbano, A.M., 2016. Mesozoic rift to post-rift tectonostratigraphy of the Sverdrup Basin, Canadian Arctic. Mar. Pet. Geol. 76, 148–158.
Harland, W.B., 1997. The Geology of Svalbard.. Geological Society, London, Memoir No. 17 The Geological Society, London, Bath. ISBN 1-897799-93-4.
Hammer, Ø., Collignon, M., Nakrem, H.A., 2012. Organic carbon isotope chemostratigraphy and cyclostratigraphy in the Volgian of Svalbard. Nor. J. Geol. 92, 103–112.
Hammer, Ø., Jones, M.T., Schneebeli-Hermann, E., Hansen, B.B., Bucher, H., 2019. Are early Triassic extinction events associated with mercury anomalies? A reassessment of the Smithian/Spathian boundary extinction. Earth Sci. Rev. 195, 179–190. https://doi.org/10.1016/j.earscirev.2019.04.016.
Hawkesworth, C.J., Gallagher, K., Kirstein, L., Mantovani, M.S.M., Peate, D.W., Turner, S.P., 2000. Tectonic controls on magmatism associated with continental break-up: an example from the Paraná-Etendeka Province. Earth Planet. Sci. Lett. 179 (2), 335–349.
Helland-Hansen, W., Grundvåg, S.A., 2021. The Svalbard Eocene-Oligocene (?) Central Basin succession: Sedimentation patterns and controls. Basin Res. 33 (1), 729–753.
Herrle, J.O., Schröder-Adams, C.J., Davis, W., Pugh, A.T., Galloway, J.M., Fath, J., 2015. Mid-cretaceous High Arctic stratigraphy, climate, and oceanic anoxic events. Geology 43 (5), 403–406.
Hlohowskyj, S.R., Chappaz, A., Dickson, A.J., 2021. Molybdenum as a Paleoredox Proxy: Past, Present, and Future. Series: Elements in Geochemical Tracers in Earth System Science. Cambridge University Press.
Hoernle, K., Hauff, F., Van den Bogaard, P., Werner, R., Mortimer, N., Geldmacher, J., Garbe-Schönberg, D., Davy, B., 2010. Age and geochemistry of volcanic rocks from the Hikurangi and Manihiki oceanic Plateaus. Geochim. Cosmochim. Acta 74 (24), 7196–7219.
Hunt, J.M., 1996. Petroleum Geochemistry and Geology, Second edition. W.H. Freeman and Company, New York.
Jelby, M.E., Śliwińska, K.K., Koevoets, M.J., Alsen, P., Vickers, M.L., Olaussen, S., Stemmerik, L., 2020a. Arctic reappraisal of global carbon-cycle dynamics across the Jurassic-cretaceous boundary and Valanginian Weissert Event. Palaeogeogr. Palaeoclimatol. Palaeoecol. 555, 109847.
Jelby, M.E., Grundvåg, S.-A., Helland-Hansen, W., Olaussen, S., Stemmerik, L., 2020b. Tempestite facies variability and storm-depositional processes across a wide ramp: Towards a polygenetic model for hummocky cross-stratification. Sedimentology 67, 742–781.
Jenkyns, H.C., 1995. Carbon-isotope stratigraphy and paleoceanographic significance of the Lower Cretaceous shallow-water carbonates of Resolution Guyot, Mid-Pacific Mountains.. In: Proceedings of the Ocean Drilling Program, Scientific Results, pp. 99–104.
Jenkyns, H.C., 1980. Cretaceous anoxic events: from continents to oceans. J. Geol. Soc. 137 (2), 171–188.
Johnsen, S.O., Mørk, A., Dypvik, H., Nagy, J., 2001. Outline of the Geology of Svalbard, short geological review and guidebook. In: 7th ESF IMPACT Workshop, 11.
Jones, M.T., Jerram, D.A., Svensen, H.H., Grove, C., 2016. The effects of large igneous provinces on the global carbon and Sulphur cycles. Palaeogeogr. Palaeoclimatol. Palaeoecol. 441, 4–21.
Jones, C.E., Jenkyns, H.C., Coe, A.L., Stephen, H.P., 1994. Strontium isotopic variations in Jurassic and cretaceous seawater. Geochim. Cosmochim. Acta 58 (14), 3061–3074.
Jones, C.E., Jenkyns, H.C., 2001. Seawater strontium isotopes, oceanic anoxic events, and seafloor hydrothermal activity in the Jurassic and cretaceous. Am. J. Sci. 301 (2), 112–149.
Kerr, A.C., Mahoney, J.J., 2007. Oceanic plateaus: Problematic plumes, potential paradigms. Chem. Geol. 241 (3–4), 332–353.
Kasbohm, J., Schoene, B., Burgess, S., 2021. Radiometric constraints on the timing, tempo, and effects of large igneous province emplacement. In: Ernst, R.E., Dickson, A.J., Bekker, A. (Eds.), Large Igneous Provinces: A Driver of Global Environmental and Biotic Changes. American Geophysical Union and John Wiley and Sons, Inc, pp. 27–82.
Koevoets, M.J., Hammer, O., Olaussen, S., Senger, K., Smelror, M., 2018. Integrating subsurface and outcrop data of the Middle Jurassic to lower cretaceous Agardhfjellet Formation in Central Spitsbergen. Nor. J. Geol. 99, 219–252.
Koevoets, M.J., Abay, T.B., Hammer, Ø., Olaussen, S., 2016. High-resolution organic carbon–isotope stratigraphy of the Middle Jurassic-lower cretaceous Agardhfjellet

Formation of Central Spitsbergen, Svalbard. Palaeogeogr. Palaeoclimatol. Palaeoecol. 449, 266–274. https://doi.org/10.1016/j.palaeo.2016.02.029.
Lafargue, E., Marquis, F., Pillot, D., 1998. Rock-Eval 6 applications in hydrocarbon exploration, production, and soil contamination studies. Rev. l'Inst. Français Pétrole 53, 421–437.
Littler, K., Robinson, S.A., Bown, P.R., Nederbragt, A.J., Pancost, R.D., 2011. High sea-surface temperatures during the Early Cretaceous Epoch. Nature Geoscience 4 (3), 169–172.
Lundin, E.R., Dore, A.G., 1997. A tectonic model for the norwegian passive margin with implications for the NE Atlantic: early cretaceous to break-up. J. Geol. Soc. 154 (3), 545–550.
Lyons, T.W., Anbar, A.D., Severmann, S., Scott, C., Gill, B.C., 2009. Tracking Euxinia in the Ancient Ocean: a Multiproxy Perspective and Proterozoic Case Study. Annu. Rev. Earth Planet. Sci. 37, 507–534.
Maher, H.D., 2001. Manifestations of the cretaceous High Arctic large igneous province in Svalbard. J. Geol. 109 (1), 91–104.
Mahoney, J.J., Storey, M., Duncan, R.A., Spencer, K.J., Pringle, M., 1993. Geochemistry and age of the Ontong Java Plateau. In: The Mesozoic Pacific: Geology, Tectonics, and Volcanism, 77, pp. 233–261.
Mahoney, J.J., Duncan, R.A., Tejada, M.L.G., Sager, W.W., Bralower, T.J., 2005. Jurassic-cretaceous boundary age and mid-ocean-ridge–type mantle source for Shatsky rise. Geology 33 (3), 185–188.
Martinez, M., Deconinck, J.-F., Pellenard, P., Riquier, L., Company, M., Reboulet, S., Moiroud, M., 2015. Astrochronology of the Valanginian-Hauterivian stages (Early Cretaceous): Chronological relationships between the Paraná-Etendeka large igneous province and the Weissert and the Faraoni events. Glob. Planet. Chang. 131, 158–173.
Martínez-Rodríguez, R., Selby, D., Castro, J.M., de Gea, G.A., Nieto, L.M., Ruiz-Ortiz, P. A., 2021. Tracking magmatism and oceanic change through the early Aptian Anoxic Event (OAE 1a) to the late Aptian: Insights from osmium isotopes from the westernmost Tethys (SE Spain) Cau Core. Glob. Planet. Chang. 207, 103652.
McArthur, J., Janssen, N., Reboulet, S., Leng, M., Thirlwall, M., Van de Schootbrugge, B., 2007. Palaeotemperatures, Polar ice-volume, and isotope stratigraphy (Mg/Ca, δ18O, δ13C, 87Sr/86Sr): The Early Cretaceous (Berriasian, Valanginian, Hauterivian). Palaeogeography, Palaeoclimatology, Palaeoecology 248 (3), 391–430.
Menegatti, A.P., Weissert, H., Brown, R.S., Tyson, R.V., Farrimond, P., Strasser, A., Caron, M., 1998. High-resolution δ13C stratigraphy through the early Aptian "Livello selli" of the Alpine Tethys. Paleoceanography 13 (5), 530–554.
Midtkandal, I., Faleide, J.I., Faleide, T.S., Serck, C.S., Planke, S., Corseri, R., Dimitriou, M., Nystuen, J.P., 2020. Lower cretaceous Barents Sea strata: epicontinental basin configuration, timing, correlation and depositional dynamics. Geol. Mag. 157 (3), 458–476.
Midtkandal, I., Svensen, H.H., Planke, S., Corfu, F., Polteau, S., Torsvik, T.H., Faleide, J. I., Grundvåg, S.A., Selnes, H., Kürschner, W., Olaussen, S., 2016. The Aptian (Early Cretaceous) oceanic anoxic event (OAE1a) in Svalbard, Barents Sea, and the absolute age of the Barremian-Aptian boundary. Palaeogeogr. Palaeoclimatol. Palaeoecol. 463, 126–135.
Midtkandal, I., Nystuen, J., 2009. Depositional architecture of a low-gradient ramp shelf in an epicontinental sea: the lower cretaceous of Svalbard. Basin Res. 21 (5), 655–675.
Mørk, A., Dallmann, W.K., Dypvik, H., Johannessen, E.P., Larssen, G.B., Nagy, J., Nøttvedt, A., Olaussen, S., Pčelina, T.M., Worsley, D., 1999. Mesozoic lithostratigraphy. In: Dallmann, W.K. (Ed.), Lithostratigraphic Lexicon of Svalbard. Norwegian Polar Institute, Tromsø.
Mutterlose, J., Pauly, S., Steuber, T., 2009. Temperature controlled deposition of early cretaceous (Barremian–early Aptian) black shales in an epicontinental sea. Palaeogeogr. Palaeoclimatol. Palaeoecol. 273 (3), 330–345.
Naber, T.V., Grasby, S.E., Cuthbertson, J.P., Rayner, N., Tegner, C., 2021. New constraints on the age, geochemistry, and environmental impact of High Arctic Large Igneous Province magmatism: Tracing the extension of the Alpha Ridge onto Ellesmere Island, Canada. GSA Bulletin 133 (7–8), 1695–1711.
Nejbert, K., Krajewski, K.P., Dubińska, E., Pécskay, Z., 2011. Dolerites of Svalbard, north-West Barents Sea Shelf: age, tectonic setting and significance for geotectonic interpretation of the High-Arctic large Igneous Province. Polar Res. 30, 7306.
Nunn, E.V., 2007. Late Jurassic to early cretaceous stable isotope and geochemical records from the northern high latitudes: implications for palaeoclimate. University of Plymouth. PhD thesis.
Olaussen, S., Grundvåg, S.A., Senger, K., Anell, I., Betlem, P., Birchall, T., Braathen, A., Dallmann, W., Jochmann, M., Johannessen, E.P., Lord, G., 2022. The Svalbard Carboniferous to Cenozoic Composite Tectono-stratigraphic element. Geol. Soc. Lond. Mem. 57 (1), M57–M2021.
Parkinson, I.J., Schaefer, B.F., Arculus, R.J., 2002. A lower mantle origin for the world's biggest LIP? A high precision Os isotope isochron from Ontong Java Plateau basalts drilled on ODP Leg 192. Geochim. Cosmochim. Acta 66 (15A), A580.
Peate, D.W., 1997. The parana-etendeka province. In: Geophysical Monograph-American Geophysical Union, 100, pp. 217–246.
Percival, L.M., Bergquist, B.A., Mather, T.A., Sanei, H., 2021b. Sedimentary mercury enrichments as a tracer of Large Igneous Province volcanism. In: Large Igneous Provinces: A Driver of Global Environmental and Biotic Changes, pp. 247–262.
Percival, L.M., Jenkyns, H.C., Mather, T.A., Dickson, A.J., Batenburg, S.J., Ruhl, M., Hesselbo, S.P., Barclay, R., Jarvis, I., Robinson, S.A., Woelders, L., 2018. Does large igneous province volcanism always perturb the mercury cycle? Comparing the records of Oceanic Anoxic event 2 and the end-cretaceous to other Mesozoic events. Am. J. Sci. 318 (8), 799–860.
Percival, L.M., Ruhl, M., Hesselbo, S.P., Jenkyns, H.C., Mather, T.A., Whiteside, J.H., 2017. Mercury evidence for pulsed volcanism during the end-Triassic mass extinction. Proc. Natl. Acad. Sci. 114 (30), 7929–7934.
Percival, L.M.E., Tedeschi, L.R., Creaser, R.A., Bottini, C., Erba, E., Giraud, F., Svensen, H., Savian, J., Trindade, R., Coccioni, R., Frontalini, F., 2021a. Determining the style and provenance of magmatic activity during the Early Aptian Oceanic Anoxic Event (OAE 1a). Global and Planetary Change 200, 103461.
Polteau, S., Hendriks, B.W., Planke, S., Ganerød, M., Corfu, F., Faleide, J.I., Midtkandal, I., Svensen, H.S., Myklebust, R., 2016. The early cretaceous Barents Sea Sill complex: distribution, 40Ar/39Ar geochronology, and implications for carbon gas formation. Palaeogeogr. Palaeoclimatol. Palaeoecol. 441, 83–95.
Price, G.D., Főzy, I., Pálfy, J., 2016. Carbon cycle history through the Jurassic-cretaceous boundary: a new global δ13C stack. Palaeogeogr. Palaeoclimatol. Palaeoecol. 451, 46–61.
Price, G.D., 2003. New constraints upon isotope variation during the early cretaceous (Barremian–Cenomanian) from the Pacific Ocean. Geol. Mag. 140 (05), 513–522.
Robinson, S.A., Heimhofer, U., Hesselbo, S.P., Petrizzo, M.R., 2017. Mesozoic climates and oceans–a tribute to Hugh Jenkyns and Helmut Weissert. Sedimentology 64 (1), 1–15.
Price, G.D., Passey, B.H., 2013. Dynamic polar climates in a greenhouse world: Evidence from clumped isotope thermometry of Early Cretaceous belemnites. Geology 41 (8), 923–926.
Robinson, S.A., Clarke, L.J., Nederbragt, A., Wood, I.G., 2008. Mid-cretaceous oceanic anoxic events in the Pacific Ocean revealed by carbon-isotope stratigraphy of the Calera Limestone, California, USA. Geol. Soc. Am. Bull. 120 (11–12), 1416–1426.
Rocha, B.C., Davies, J.H., Janasi, V.A., Schaltegger, U., Nardy, A.J., Greber, N.D., Lucchetti, A.C.F., Polo, L.A., 2020. Rapid eruption of silicic magmas from the Paraná magmatic province (Brazil) did not trigger the Valanginian event. Geology 48 (12), 1174–1178. https://doi.org/10.1130/G47766.1.
Sager, W.W., Zhang, J., Korenaga, J., Sano, T., Koppers, A.A., Widdowson, M., Mahoney, J.J., 2013. An immense shield volcano within the Shatsky rise oceanic plateau, Northwest Pacific Ocean. Nat. Geosci. 6 (11), 976–981.
Sanei, H., Grasby, S.E., Beauchamp, B., 2012. Latest permian mercury anomalies. Geology 40 (1), 63–66.
Sanei, H., Grasby, S.E., Beauchamp, B., 2015. Contaminants in marine sedimentary deposits from coal fly ash during the Latest Permian Extinction. In: Blais, J.M., Rosen, M.R., Smol, J.P. (Eds.), Environmental Contaminants: Using Natural Archives to Track Sources and Long-term Trends of Pollution, Series: Developments in Paleoenvironmental Research, Vol. 18. Springer, Dordrecht, 547, 89-99.
Sanei, H., Outridge, P.M., Oguri, K., Stern, G.A., Thamdrup, B., Wenzhöfer, F., Wang, F., Glud, R.N., 2021. High mercury accumulation in deep-ocean hadal sediments. Sci. Rep. 11 (1), 1–8.
Scaife, J.D., Ruhl, M., Dickson, A.J., Mather, T.A., Jenkyns, H.C., Percival, L.M.E., Hesselbo, S.P., Cartwright, J., Eldrett, J.S., Bergman, S.C., Minisini, D., 2017. Sedimentary mercury enrichments as a marker for submarine large igneous province volcanism? Evidence from the Mid-Cenomanian event and Oceanic Anoxic Event 2 (Late Cretaceous). Geochem. Geophys. Geosyst. 18 (12), 4253–4275.
Schlanger, S.O., Jenkyns, H.C., Premoli-Silva, I., 1981. Volcanism and vertical tectonics in the Pacific Basin related to global cretaceous transgressions. Earth Planet. Sci. Lett. 52 (2), 435–449.
Senger, K., Tveranger, J., Ogata, K., Braathen, A., Planke, S., 2014. Late Mesozoic magmatism in Svalbard: a review. Earth Sci. Rev. 139, 123–144.
Sliter, W.V., 1989. Aptian anoxia in the Pacific Basin. Geology 17 (10), 909–912.
Śliwińska, K.K., Jelby, M.E., Grundvåg, S.-A., Nøhr-Hansen, H., Alsen, P., Olaussen, S., 2020. Dinocyst stratigraphy of the Valanginian-Aptian Rurikfjellet and Helvetiafjellet formations on Spitsbergen, Arctic Norway. Geol. Mag. 157, 1693–1714. https://doi.org/10.1017/S0016756819001249.
Storm, M.S., Hesselbo, S.P., Jenkyns, H.C., Ruhl, M., Ullmann, C.V., Xu, W., Leng, M.J., Riding, J.B., Gorbanenko, O., 2020. Orbital pacing and secular evolution of the early Jurassic carbon cycle. Proc. Natl. Acad. Sci. 117 (8), 3974–3982.
Suan, G., Van De Schootbrugge, B., Adatte, T., Fiebig, J., Oschmann, W., 2015. Calibrating the magnitude of the Toarcian carbon cycle perturbation. Paleoceanography 30, 495–509.
Tarduno, J., Mayer, H., Winterer, E., Sliter, W., Kroenke, L., Mahoney, J., Leckie, M., Musgrave, R., Storey, M., 1991. Rapid formation of Ontong Java Plateau by Aptian mantle plume volcanism. Science 254 (5030), 399–403.
Tejada, M.L.G., Suzuki, K., Kuroda, J., Coccioni, R., Mahoney, J.J., Ohkouchi, N., Sakamoto, T., Tatsumi, Y., 2009. Ontong Java Plateau eruption as a trigger for the early Aptian oceanic anoxic event. Geology 37 (9), 855–858.
Taylor, B., 2006. The single largest oceanic plateau: Ontong Java–Manihiki–Hikurangi. Earth Planet. Sci. Lett. 241 (3–4), 372–380.
Tejada, M., Mahoney, J., Neal, C., Duncan, R., Petterson, M., 2002. Basement geochemistry and geochronology of Central Malaita, Solomon Islands, with implications for the origin and evolution of the Ontong Java Plateau. J. Petrol. 43 (3), 449–484.
Them II, T.R., Jagoe, C.H., Caruthers, A.H., Gill, B.C., Grasby, S.E., Gröcke, D.R., Yin, R., Owens, J.D., 2019. Terrestrial sources as the primary delivery mechanism of mercury to the oceans across the Toarcian Oceanic Anoxic Event (Early Jurassic). Earth Planet. Sci. Lett. 507, 62–72. https://doi.org/10.1016/j.epsl.2018.11.029.
Torsvik, T.H., Carlos, D., Mosar, J., Cocks, L.R.M., Malme, T.N., 2002. Global reconstructions and North Atlantic paleogeography 440 Ma to recent. In: BATLAS—Mid Norway Plate Reconstruction Atlas with Global and Atlantic Perspectives, pp. 18–39.
Thordarson, T., 2004. Accretionary-lapilli-bearing pyroclastic rocks at ODP Leg 192 Site 1184: a record of subaerial phreatomagmatic eruptions on the Ontong Java Plateau. Geol. Soc. Lond., Spec. Publ. 229 (1), 275–306.

Tribovillard, N., Algeo, T.J., Lyons, T., Riboulleau, A., 2006. Trace metals as paleoredox and paleoproductivity proxies: an update. Chem. Geol. 232 (1–2), 12–32.
Tyson, R.V., 1995. Sedimentary Organic Matter. Chapman and Hall, London.
Vickers, M.L., Price, G.D., Jerrett, R.M., Sutton, P., Watkinson, M.P., FitzPatrick, M., 2019. The duration and magnitude of cretaceous cool events: evidence from the northern high latitudes. Bulletin 131 (11–12), 1979–1994.
Vickers, M.L., Price, G.D., Jerrett, R.M., Watkinson, M., 2016. Stratigraphic and geochemical expression of Barremian-Aptian global climate change in Arctic Svalbard. Geosphere 12 (5), 1594–1605.
Waichel, B.L., Scherer, C.M., Frank, H.T., 2008. Basaltic lava flows covering active aeolian dunes in the Paraná Basin in southern Brazil: Features and emplacement aspects. J. Volcanol. Geotherm. Res. 171, 59–72.
Weissert, H., Lini, A., Föllmi, K.B., Kuhn, O., 1998. Correlation of early cretaceous carbon isotope stratigraphy and platform drowning events: a possible link? Palaeogeogr. Palaeoclimatol. Palaeoecol. 137 (3), 189–203.
Weissert, H., Erba, E., 2004. Volcanism, CO2 and palaeoclimate: a late Jurassic-early cretaceous carbon and oxygen isotope record. J. Geol. Soc. 161 (4), 695–702.